ISSN 0024-4902, Lithology and Mineral Resources, 2006, Vol. 41, No. 6, pp. 547–569. © Pleiades Publishing, Inc., 2006.
Original Russian Text © T.A. Ivanovskaya, N.V. Gor'kova, G.V. Karpova, E.V. Pokrovskaya, 2006, published in Litologiya i Poleznye Iskopaemye, 2006, No. 6, pp. 611–634.

Phyllosilicates (Glauconite, Illite, and Chlorite) in Terrigenous Sediments of the Arymas Formation (Olenek High)

T. A. Ivanovskaya, N. V. Gor'kova, G. V. Karpova, and E. V. Pokrovskaya

Geological Institute, Russian Academy of Sciences, Pyzhevskii per. 7, Moscow, 119017 Russia

e-mail: semikhatov@ginras.ru

Received May 29, 2006

Abstract—It is shown that globular phyllosilicates subjected to deep catagenesis are abundant in Middle Riphean sandstones and siltstones (lower subformation of the Arymas Formation) of the Olenek High. Their detailed structural–crystallochemical characteristics are given. Secondary alterations of globules and the associated pelletal minerals at different stages of lithogenesis (illitization, chloritization, ferrugination, disintegration, and so on) are considered. Structural–crystallochemical characteristics of Fe-illite and Fe^{2+}–Mg-chlorite in globules, pellets, separate clayey strata among glauconite-bearing sandstones and siltstones (hereafter, sandy–silty rocks), and mudstone interlayers are also presented. Possible mechanisms of the formation of these minerals are discussed.

DOI: 10.1134/S0024490206060046

INTRODUCTION

At present, lithological–mineralogical and structural–crystallochemical (including the Mössbauer) investigations of globular phyllosilicates of the glauconite series and their host rocks are essential for the isotope–geochronological implications.

The present communication reports results of the first stage of investigation. We analyzed the mineralogical and structural–crystallochemical features of the globular phyllosilicates, including their diverse secondary alterations (illitization, chloritization, ferrugination, and disintegration). We also examined the enclosing rocks. Results of the Mössbauer and isotope–geochronological investigations will be discussed in the next communication.

In the previous investigation of glauconite chloritization, we described the partial replacement of the globular and pelletal Al-glauconite by Fe^{2+}–Mg-chlorite in sandstones subjected to deep catagenesis (Pärä-jarvi Formation, Upper Riphean, Srednii Peninsula) (Ivanovskaya et al., 2003). This process is very weakly developed in the glauconite-bearing sandy–silty rocks of the Arymas Formation. Here, we see a different situation: at separate horizons of the studied sections, some glauconite globules and flakes are observed as differently illitized (up to the point of complete pseudomorphoses in some places) brownish segregations that are later subjected to partial chloritization at both microscopic and macroscopic levels. Complete chloritization is developed in mudstones and, partially, clayey strata in the sandy–silty rocks.

Chloritization of glauconite globules and pelletal minerals related to the local heating of glauconite-bearing rocks at the contact with intrusive rocks (Kotuikan Formation, Lower Riphean, Anabar Massif) is scrutinized in (Drits et al., 2001). The Arymas subformation section also shows the local chloritization of globular and pellets of the glauconite–illite composition.

As is known, chlorites and illites are common in association with other minerals. Therefore, it is rather difficult to determine their chemical composition. However, the presence of virtually monomineral illite segregations in the study region made it possible to solve the problems formulated above.

Thus, the present work is devoted to the detailed mineralogical and structural–crystallochemical investigation of dioctahedral phyllosilicates (glauconite–illite series) and trioctahedral chlorites, as well as the discussion of their genetic features.

OBJECTS

The Middle Riphean age of the Arymas Formation was traditionally based on the succession of stromatolitic associations in Riphean rocks of the Olenek High (Komar, 1966; Shpunt et al., 1982; Semikhatov and Serebryakov, 1983) and the K–Ar datings obtained in the 1960s for the mineralogically unexplored glauconites in terrigenous rocks of the Arymas Formation (*Geokhronologiya…,* 1968).

The Arymas Formation is widespread on the southern slope of the Olenek High as a NE-striking zone 3–7 km wide and ~65 km long. Rocks of this formation make up a NW-inclined gentle monocline complicated by faults. They are universally separated from the underlying Kyutingda Formation (Lower Riphean) by a sill of Upper Proterozoic diabases and conformably overlain by glauconite-bearing sandy–silty rocks of the

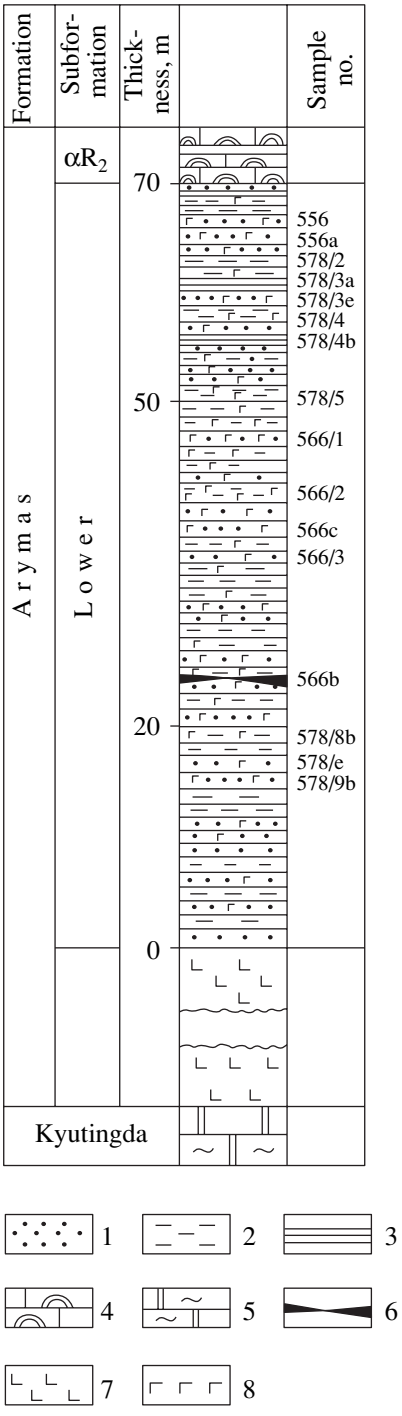

Fig. 1. Schematic section of the lower subformation of the Arymas Formation. (1) Sandstones; (2) siltstones; (3) mudstones; (4) limestones; (5) dolomites; (6) glauconitite interlayer; (7) diabases; (8) glauconite.

Debengda Formation. Despite the unclear contact, many researchers believe that these formations are conformable (Komar, 1966; Kats and Florova, 1986; Shenfil, 1991).

In the majority of sections, the Arymas Formation is divided into two sequences (subformations) interrelated by gradual transitions. The lower subformation is composed of terrigenous rocks, whereas the upper subformation is dominated by carbonates. The terrigenous subformation consists of fine-grained glauconite sandy–silty rocks with rare mudstone units. The carbonate subformation is composed of bioherm (stromatolitic) limestones and dolomites separated by mudstone and siltstone interlayers. The total thickness of the formation is 250–290 m. However, estimates of the thickness of separate subformations are different. According to some researchers, the lower subformation is 70 m thick, whereas the upper subformation is 200 m thick (Komar, 1966). According to (Kats and Florova, 1986; Shenfil et al., 1988), the thickness of the terrigenous and carbonate subformations is 130–150 and 140 m, respectively. Without going into discussion concerning the reason of such discrepancies, let us note the following fact. In 1987–1989, Ivanovskaya, Florova, and Kats investigated one of the reference sections of the Arymas Formation exposed 5.5 km upward the mouth of the Debengda River. At that time, the thickness of the lower subformation was estimated at ~70 m. Ivanovskaya investigated an additional section of the lower subformation in the southwestern area exposed 40 km away from the above site on the right bank of the Ulakhan-Sololi River located 6.5 km upward the river mouth. This section only showed upper units of the lower subformation and their thickness did not exceed 10 m.

Based on the glauconite content, sandy–silty rocks of the lower subformation in the Debengda section can be divided into three units, among which the middle unit (~30 m) shows the highest glauconite content. The glauconite content is insignificant in the lower and upper units.

In the studied sandy–silty section, the most typical varieties are confined to the upper (samples 578/2, 578/3e, 578/4, 578/5), middle (samples 566/1, 566/2, 566c, 566/3, 566b), and lower (samples 578/8b, 578/8e, 578/9b) units. Sample 581b was taken from the roof of the upper unit at the contact of a diabase stock with the glauconite-bearing siltstones.

Glauconite is absent in rare mudstone interlayers confined to the upper unit. The mudstone interlayers are almost completely composed of chlorite (samples 578/3a, 578/4b). Therefore, we carried out their detailed examination.

In the Ulakhan-Sololi section, upper units of the lower subformation are represented by samples 556 and 556a taken from the middle part of the 10-m-thick section. They consist of sandy–silty rocks that are enriched in glauconite, relative to the Debengda counterpart.

Positions of all samples studied are shown in the schematic section of the lower subformation of the Arymas Formation (Fig. 1).

METHODS

Monomineral fractions of glauconite grains were extracted by the routine procedure: crushing (excluding the loose sample 566b), sieving, and separation of grain size fractions with SEM-1 and SIM-1 electromagnets. If the material was sufficient (samples 556, 566/1, 566/2), the fractions were separated in terms of density ranging from 2.6 to >2.9 g/cm^3 (spacing 0.05 g/cm^3) and further subjected to ultrasonic purification. At the final stage of sample preparation, the extracted grains were additionally purified by a needle under binocular microscope.

The grains and rocks, in general, were studied with optical (including scanning electron microscopy), X-ray, and microprobe methods.

X-ray investigations were carried out with DRON-2 and DRON-4-13 diffractometers using CuKα radiation. Diffraction curves were recorded in both continuous and discrete regimes.

The quantitative microprobe analysis with Cameca was performed for separate grains placed in a pellet and for different materials in polished sections. The qualitative microprobe analysis of different materials was accomplished with a Camscan MV-2300 scanning electron microscope equipped with an Oxford-Instruments device. Calculations were performed using the INCA-250 software, which adjusts the sum total of oxides to 100% without the consideration of water.

We also recorded X-ray characteristics for minerals associated with glauconite (including the clayey phases). The clayey fractions (from 0.6 to 5 μm in size) were decanted from the glauconite-bearing and enclosing rocks along the whole subformation section.

The detailedness of sample investigation depended on the quantity of material and the formulated task. Let us emphasize that we often analyzed different materials (globules, flakes of various colors and compositions, chlorite patches, clayey component, and so on) in a single sample with the same number.

RESULTS

Characteristics of Rocks

In the studied sections, rocks of the lower subformation of the Arymas Formation are represented by various proportions of fine-grained sandstones, siltstones, and mudstones. The sections are dominated by siltstones. As mentioned above, mudstones are mainly developed as a subordinate component in the upper unit of the subformation.

The *sandy–silty rocks* are usually fine-layered, laminated, and, less commonly, massive formations that are characterized by pale and dark gray colors of various (greenish, pinky, yellowish, and so on) tints.

The rocks are composed of quartz and feldspar–quartz aggregates with a variable content of clays and glauconite. They also contain numerous greenish brown, brown, green, and colorless flakes, as well as Ti-bearing minerals (leucoxene and anatase), hematite, iron hydroxides, and occasional unoxidized pyrite. Accessory minerals are represented by amphiboles, zircon, and tourmaline.

Cement in the rocks is composed of clay (interstitial and basal), chlorite (interstitial, pellicular, and crustification), glauconite (interstitial), hydromica (pellicular), feldspar–quartz (conformal-regeneration), less common hematite (interstitial and pellicular), and rare calcite (interstitial) materials. In some interlayers and/or sectors, the rocks are dominated by the interstitial–pellicular cement, while the conformal-regeneration texture prevails in other sectors with a minor content of the clayey component.

In sandy–silty interlayers of the upper unit of the subformation exposed in two sections (samples 556a, 578/2, 578/3e, 578/4), the clayey substance makes up not only the interstitial matrix, but also separate strata, lenticles, and patches of various shapes (hereafter, strata). The clayey substance has a brownish color, fine-dispersed texture, and high values of refractive index and interference ranging from dark gray to yellowish orange shades.

In some places, the brownish clayey material is partly transformed into light green chlorite with a lower (or anomalous) birefringence and higher refractive index, relative to the parental clayey material (Fig. 2a). Chlorite makes up diverse (in shape and size) patches and differently crystallized segregations in veins. In some cases, chlorite flakes are hardly discernible, whereas they are up to 0.02 mm in size in other cases. The arrangement of flakes can be random or subparallel. However, they often make up sheaflike aggregates that can be transformed into spherulitic structures, which are typical of large chlorite aggregates containing the authigenic quartz and hematite flakes.

In some places, the brownish clayey material contains an admixture of fine-grained (0.1–0.01 mm along the long axis) dark or pale greenish brown and brown flakes resembling biotite in terms of optical properties. However, they are often characterized by obscure shape, weak pleochroism, and lower interference.

Large brown, colorless, and green flakes (up to 0.6–0.1 mm along the long axis) occur as separate segregations at several stratigraphic levels of the subformation. The colorless and brown varieties are similar to muscovite and biotite, respectively, in terms of optical properties. As is known, muscovite is well preserved. Based on microprobe data, the composition of one colorless flake fits the monomineral Fe-muscovite. Its crystallochemical formula is given below.

Brown flakes show different degrees of alteration. In addition to well-preserved varieties, deformed and partially amorphous segregations with split edges are also observed. In some places, they occur as fan-shaped flakes. Some flakes contain quartz rim along the cleav-

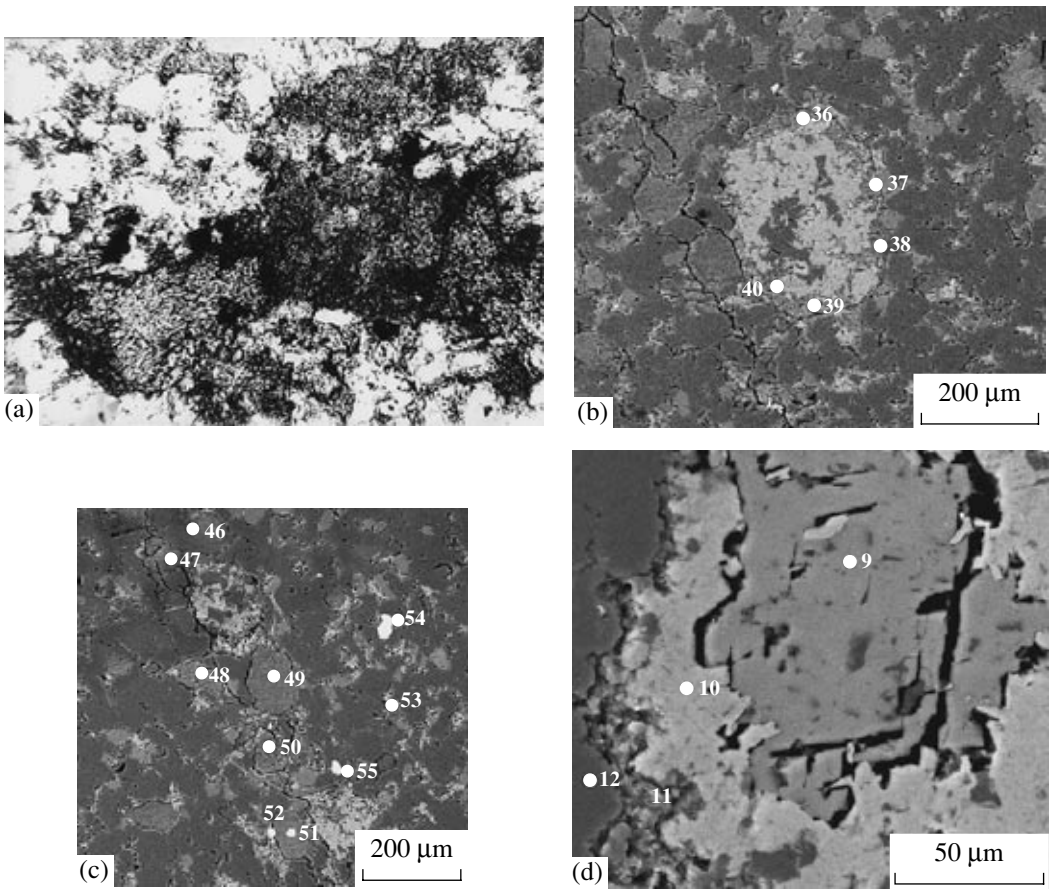

Fig. 2. Photomicrographs of glauconite siltstones. (a–c) Sample 578/4; (d) sample 578/3e. (a) Sector of clayey stratum partly transformed into chlorite (pale patches among the darker clayey matrix), thin section, magn. ~80. (b, c) Camscan SEM image taken in thin section (semiquantitative analysis): (b) brownish grain partly replaced by chlorite (pale) containing authigenic quartz (dark); (36–40) analysis numbers: (39) Fe-illite, (36–38, 40) Fe-illite and chlorite blend; (c) brownish grains (analyses 46–51) chloritized in some places, chloritic pore cement (analyses 52, 53), and zircon inclusions (analyses 54, 55). (d) At the contact with quartz (analysis 12), some part of the clayey stratum (analysis 11) is almost completely replaced by chlorite (analysis 10) and calcite (analysis 9).

age and often include Ti-bearing minerals (leucoxene and anatase) and hematite crystallites.

The brown flakes are composed of different minerals: chloritized and illitized trioctahedral phyllosilicates of the biotite–phlogopite series, monomineral Fe-illite, and mixture of illite and chlorite in different proportions.

Chlorite as pellicular and interstitial cement is widespread in the subformation. The mineral is characterized by light green color with various shades, high refractive index, and low and/or anomalous birefringence. The interstitial chlorite is developed as structureless phase or flakes among the structureless matrix. In some places, chlorite flakes make up a crustification rim around clastic grains (sample 578/9b).

Chlorite corrodes and replaces to a variable extent quartz, feldspars, clayey material, and pelletal minerals of different colors.

Glauconite globules are distributed in rocks randomly and/or along layers. Their content varies from 1–2 to 15–20% and reaches 50% or more in rare cases (sample 566b). In some strata, they are deformed to a variable extent like the flakes. In rare cases, they make up peculiar festoons and matrix.

In polished sections, one can see green globules, as well as brownish green and brownish (uniformly colored or variegated) varieties (samples 556a, 578/2, 578/4, 566c). Like glauconite, they show microaggregate extinction. The interference is strong or weak.

Some brownish grains exhibit different (in shape and size) sectors filled with large sheafs and spherulitic aggregates of light green chlorite. In the polished section (sample 578/4), one can see the development of the pale chlorite among the darker (brownish) variety and interstitial matrix (Figs. 2b, 2c). At the same time, green glauconite grains in many samples from the Arymas subformation (including the samples mentioned above) contain only sporadic dissemination and fine stringers of the pale yellowish green chlorite characterized by a higher refractive index relative to the glauconite.

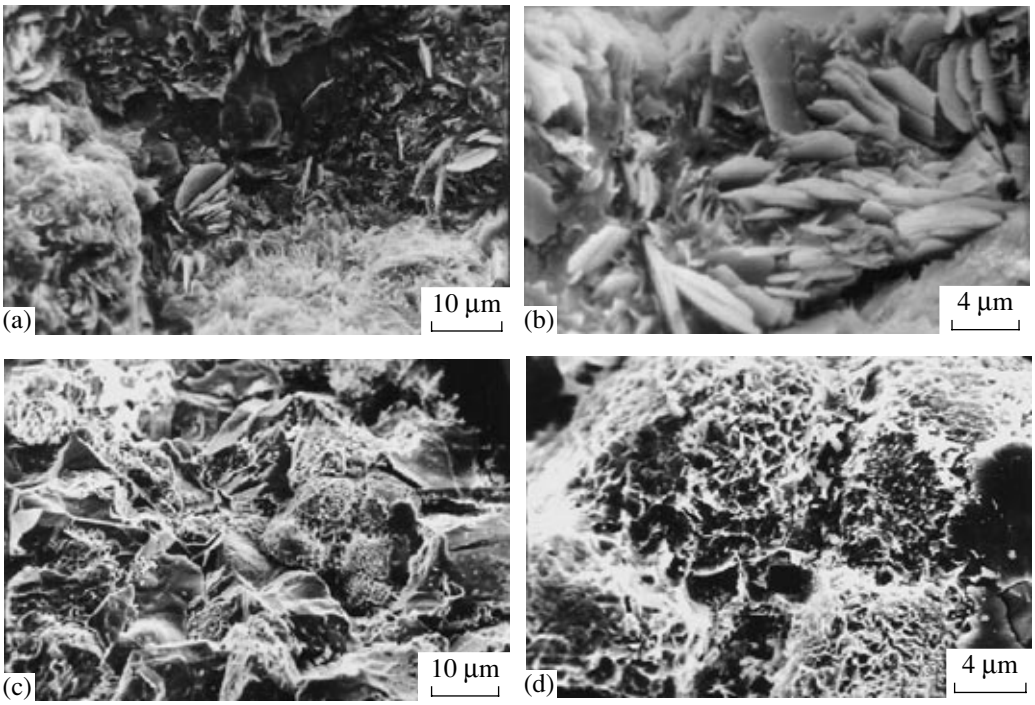

Fig. 3. Hematite microtexture. Stereoscan-600 SEM image. (a, b) Hematite crystallites in glauconite globules (sample 566b); (c) siltstone chip (sample 578/8b) with brownish red (hematitized) globules; (d) closeup of globule fragment located at the center of the right-hand sector.

The bottom of middle part of the subformation (Fig. 1) includes a glauconitite interlayer with the glauconite content of 50% or more (sample 566b). The interlayer is soft in the wet state. In the dry state, the interlayer represents a loose granular mass with sufficiently dense patches of rocks. Like the loose material, the dense patches are composed of glauconite and quartz of the sandy–silty dimension. The cement is composed of regeneration quartz, fine-dispersed glauconite, and occasional hematite.

Calcite is developed as both interstitial masses and coarse-crystalline segregations, which corrode glauconite grains and chlorite patches in the clayey strata (often, at the center), testifying to their formation at the late stage (Fig. 2d).

Hematite is developed in some interlayers of the lower part of the subformation as pellicular and interstitial cement, as well as crystalline segregations (samples 578/5, 566b, 578/8b). The hematite corrodes the ambient minerals, and they are almost completely replaced in some places. Different degrees of the replacement of glauconite by hematite in samples 566b and 578/8b are well observed in Stereoscan-600 SEM images (Fig. 3).

In globules from sample 566b, hematite makes up numerous clusters or separate crystallites of hexagonal and other shapes (Figs. 3a, 3b). Glauconite crystallites in hematite domains are very small and poorly crystallized. In sample 578/8b, the outer surface of quartz siltstone is covered with brownish red (hematitized) globules (Figs. 3c, 3d).

Mudstones were studied in two samples (578/3a and 578/4b) taken from the upper part of the subformation (Fig. 1). Sample 578/4b was taken from the glauconite-bearing sandy–silty rocks.

The pinky and/or greenish gray mudstone samples are mainly composed of chlorite. In some places (sample 578/3a), they are silicified, with a minor content of fine quartz grains and yellowish brown micaceous matrix. The latter displays red-orange interference colors. The light green chlorite is characterized by high refractive index and weak interference.

Chlorite occurs as various segregations in the studied thin sections: intricate network of flakes (sample 578/3a) and morphologically diverse segregations (sample 578/4b), including granular aggregates of rounded varieties (0.008–0.016 mm in size).

General Features of Glauconite Grains

Shape. The glauconite grains have globular (rounded, oval, strawberry-shaped, and so on), irregular, flattened (sample 556b), and occasional pelletal shapes.

Color. The grains show a wide range of green color. The lightest variety is observed in sample 578/8e; the darkest variety, in samples 556 and 566b. The bluish variety is typical of samples 556, 566/1, 566/2, and

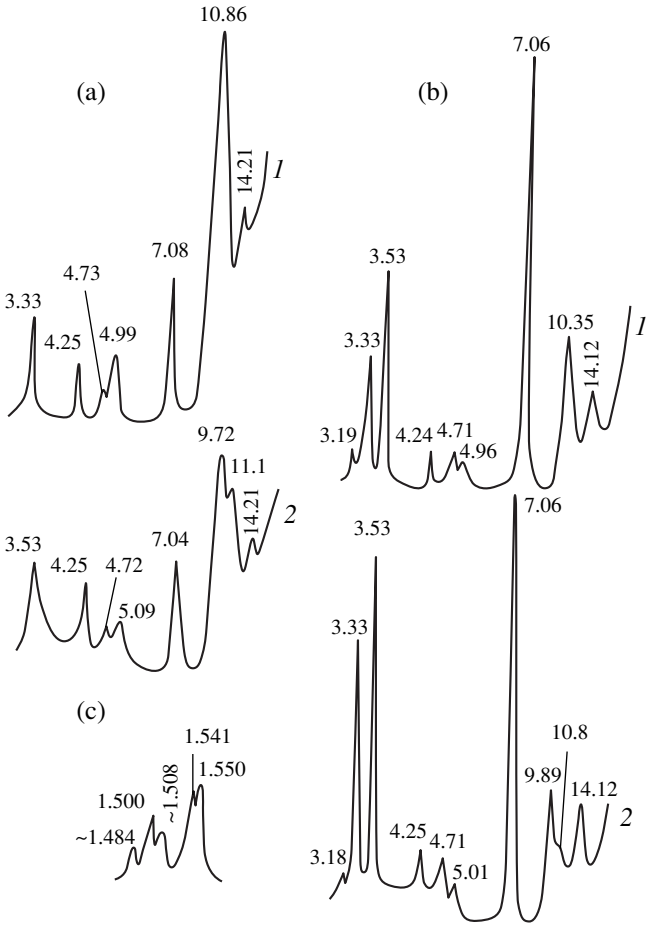

Fig. 4. Diffractograms of oriented samples of clayey fractions (<1 μm) in the (1) air-dry and (2) ethylene glycol-saturated states. (a) Sample 578/8e); (b) sample 578/2; (c) powder diffractogram. (Q) Quartz.

578/8e. In samples 556, 566/1, and 566/2 separated with respect to density, the green color intensity increases from the light fraction to heavy fractions.

Size. The size of grains ranges from 0.6 to 0.1 mm. We studied the following fractions (mm): 0.315–0.16 (samples 556, 578/4, 566/1, 566/2); 0.4–0.2 (sample 566b); 0.2–0.1 (sample 578/9b); and 0.16–0.1 (samples 578/2, 578/3e, 566c, 578/8e).

Density. The density of grains commonly ranges from 2.6–2.85 g/cm^3 (samples 556, 566/1, 566/2) to 2.65–2.75 g/cm^3 (samples 556, 566/2) and 2.7–2.8 g/cm^3 (sample 566/1).

X-Ray Characteristics of Phyllosilicates

Fine-grained component of sandy–silty rocks. X-ray study of the clayey fractions (from <0.6 to <5 μm) extracted from rocks at different levels of the subformation (samples 556, 556a, 581b, 578/2, 578/3e, 578/4, 578/5, 566/1, 566/2, 566c, 566/3, 566b, 578/8e, 578/9b) revealed the following regularity.

Diffractograms of oriented preparations of natural clayey fractions show a series of basal reflections with d(001) equal to ~10 and ~14 Å, indicating the presence of mica and chlorite minerals, respectively.

The micaceous minerals are commonly represented by hydromicas with an ordering trend in the alternation of mica and smectite layers (short-range factor, $S > 1$). This type of alternation suggests splitting of the first low-angle reflection into two reflections with d = 10.8–11.9 and 9.83–9.7 Å, respectively, in diffractograms of the ethylene glycol-saturated oriented preparations (Figs. 4a, 4b).

Relationship between intensities of mica and chlorite reflections in the majority of clayey fractions testifies to the secondary role of chlorite. Only in some samples (556a, 578/2, and 578/5), is the chlorite content commensurable with the mica component (Fig. 4b).

Nonclayey admixtures in the fractions are represented by quartz, feldspars, and occasional dolomite (samples 578/5, 578/8b, 578/8e), and calcite (samples 578/3e, 566b).

In powder diffractograms of clayey fractions, the d(060) value varies from 1.500 to 1.513 Å; parameter b, from 9.00 to 9.08 Å, respectively. Hence, the micaceous minerals correspond to dioctahedral Al–Fe-silicates. Based on the b value of 9.29 and 9.30 Å at d(060) = 1.549 and 1.550 Å, respectively, chlorite is represented by the trioctahedral Fe^{2+}–Mg-chlorite. Figure 4 shows the (060) region diffractogram of an unoriented preparation of sample 578/2 (fraction <1 μm).

Globular glauconite. Analysis of diffractograms of oriented preparations (Table 1; Figs. 5a, 5b) showed that globules are composed of hydromicas with an ordered alternation of mica and smectite layers ($S > 1$). Some samples (556a, 578/4, and 578/8e) contain traces of chlorite (Fig. 5b). The chlorite content is more appreciable in sample 578/9b. Calcite and hematite are the additional admixtures in globules from sample 566b.

It is worth mentioning that diffractograms of the natural oriented preparation of brownish red globules (sample 578/8b), which represent the complete hematite pseudomorphs of glauconite, show distinct reflections of the micaceous mineral and weak reflections of hematite. Although the hematite content is low, this mineral promotes an intense coloration of globules. However, diffraction characteristics of glauconite are not affected.

In the powder diffractograms of globules, d(060) varies from 1.506 to 1.510 Å. Parameter b of micaceous minerals varies from 9.036 and 0.06 Å (Table 1). Such b values are typical of dioctahedral micaceous minerals of the glauconite series.

Powder diffractograms of glauconite are typical of the monolayer monoclinal modifications of micas with packing defects related to the azimuthal orientation of

Table 1. X-ray data on minerals of the glauconite series

Sample no.	Grain size, mm	Grain density, g/cm^3	d(001), Å		Å	
			natural	ethylene glycol-saturated	d(060)	parameter b
556	0.315–0.16	2.65–2.75	10.60	~11; 9.83	1.5095	9.057
556a	0.2–0.16	–	10.57	10.8; 9.76	1.506	9.036
578/4	0.315–0.16	–	10.40	~11; 9.76	1.509	9.054
566/1	0.315–0.16	2.7–275	10.52	11; 9.68	1.508	9.048
566/1	0.315–0.16	2.75–2.8	10.47	11; 9.65		
566/2	0.315–0.16	2.65–2.75	10.52	11.33; 9.85	1.508	9.048
566b	0.4–0.2	–	10.40	10.8; 9.76	1.510	9.06
578/8e	0.16–0.1	–	10.94	11.05; 9.68	1.506	9.036
578/9b	0.2–0.1	–	10.70	~11.4; 9.68	1.506	9.036

Note: (–) No data.

layers as a result of their rotation by $n60°$ in 2 : 1 structures (Drits et al., 1993).

Chlorite. In clayey strata confined to siltstones (sample 578/3e), the coarse-crystalline chlorite makes up rounded and other types of dark gray segregations. In the diffractogram of oriented preparation of the dark gray sample (0.4–0.2 mm), chlorite is characterized by regular series of basal reflections with d(001) = 14.03 Å, where the intensity of even orders is much higher than that of odd ones (Fig. 5c), indicating a higher Fe content in the mineral (Bailey, 1988). Chlorite is represented by the trioctahedral Fe^{2+}–Mg variety with parameter b = 9.30 Å and d(060) = 1.550 Å.

In mudstone interlayers, chlorite associated with micaceous minerals (samples 578/4b, 578/3a) is similar to the above variety with respect to diffraction parameters (Figs. 5d, 5e). Powder diffractograms of samples 578/3a and 578/4b include reflections with d equal to ~2.68, 2.51, and 1.76 Å, suggesting the polytype modification of chlorite 1b ($\beta = 90°$) (Bailey, 1988; Drits and Kossovskaya, 1991). The Fe index of the trioctahedral Fe^{2+}–Mg-chlorite in mudstone samples is slightly different: parameter b = 9.30 and 9.33 Å at d(060) = 1.550 and 1.556 Å, respectively. This is exemplified by the powder diffractogram of sample 578/3a (Fig. 5f). As is evident, in addition to the micaceous component (b ~ 9.08 Å, d(060) = 1.514 Å), quartz is present as admixture in the mudstones.

Micaceous minerals and chlorite. Judging from the diffractograms of oriented preparations, brown pellets (sample 566/1, 0.2–0.1 mm; sample 566/3, 0.2–0.1 mm; >2.9 g/cm^3) consist of micaceous minerals and chlorite. The micaceous minerals show reflections with d(001) ~ 10.28, 4.94, and 3.35 Å (Fig.6a). The low intensity of reflection with d(002) ~ 4.94 Å indicates the presence of a high Fe content in the minerals (*Rentgenografiya...*, 1983; *Micas*, 1988). Chlorite is indicated by the nearly integer series of basal reflections with d(001) ~ 14.16 Å. Its structure is also dominated by Fe cations, as suggested by the relationship of intensities of even and odd reflections (Fig. 6a).

Diffractograms of the disordered preparation of pellets in sample 566/3 show reflections with d ~ 2.622, 2.436, 2.178, 2.014, 1.675, and 1.539 Å (Fig. 6b), suggesting that the mineral matches trioctahedral mica of the biotite–phlogopite series (*Micas*, 1988; *Mineraly*, 1992).

The powder diffractogram of sample 566/3 recorded in the discrete regime with a step of 0.02° 2θ in the 060 region demonstrates several reflections (Fig.6c). The most intense reflection (1.539 Å) corresponds to the trioctahedral micaceous mineral of the biotite–phlogopite series (b = 9.23 Å). The weaker reflection (d = 1.506 Å, b ~ 9.04 Å) suggests the presence of dioctahedral micaceous minerals of the Al–Fe composition (Al-glauconite and Fe-illite). The small bend with d ~ 1.55 Å fits the trioctahedral chlorite (b ~ 9.30 Å), which is not recorded during the continuous scanning (Fig. 6b).

Thus, the brown pellets are presumably dominated by a micaceous phase of the biotite–phlogopite (hereafter, biotite) series, while the dioctahedral micaceous minerals and trioctahedral Fe^{2+}–Mg-chlorite are present as admixtures.

Chemical Composition of Minerals

The chemical composition of mineral was studied with a Camebax microprobe. Glauconite globules placed in the pellet were analyzed in the following samples (grain size fraction and density are indicated in parentheses): 556 (0.315–0.16 mm, 2.7–2.75 g/cm^3); 578/4 (0.315–0.16 mm); 566/1 (0.315–0.16 mm, 2.7–2.8 g/cm^3); 566/2 (0.315–0.16 mm, 2.65–2.75 g/cm^3); 566b (0.4–0.2 mm); 578/9b (0.2–0.1 mm); and 578/8e (0.16–0.1 mm). Mudstones were examined in polished

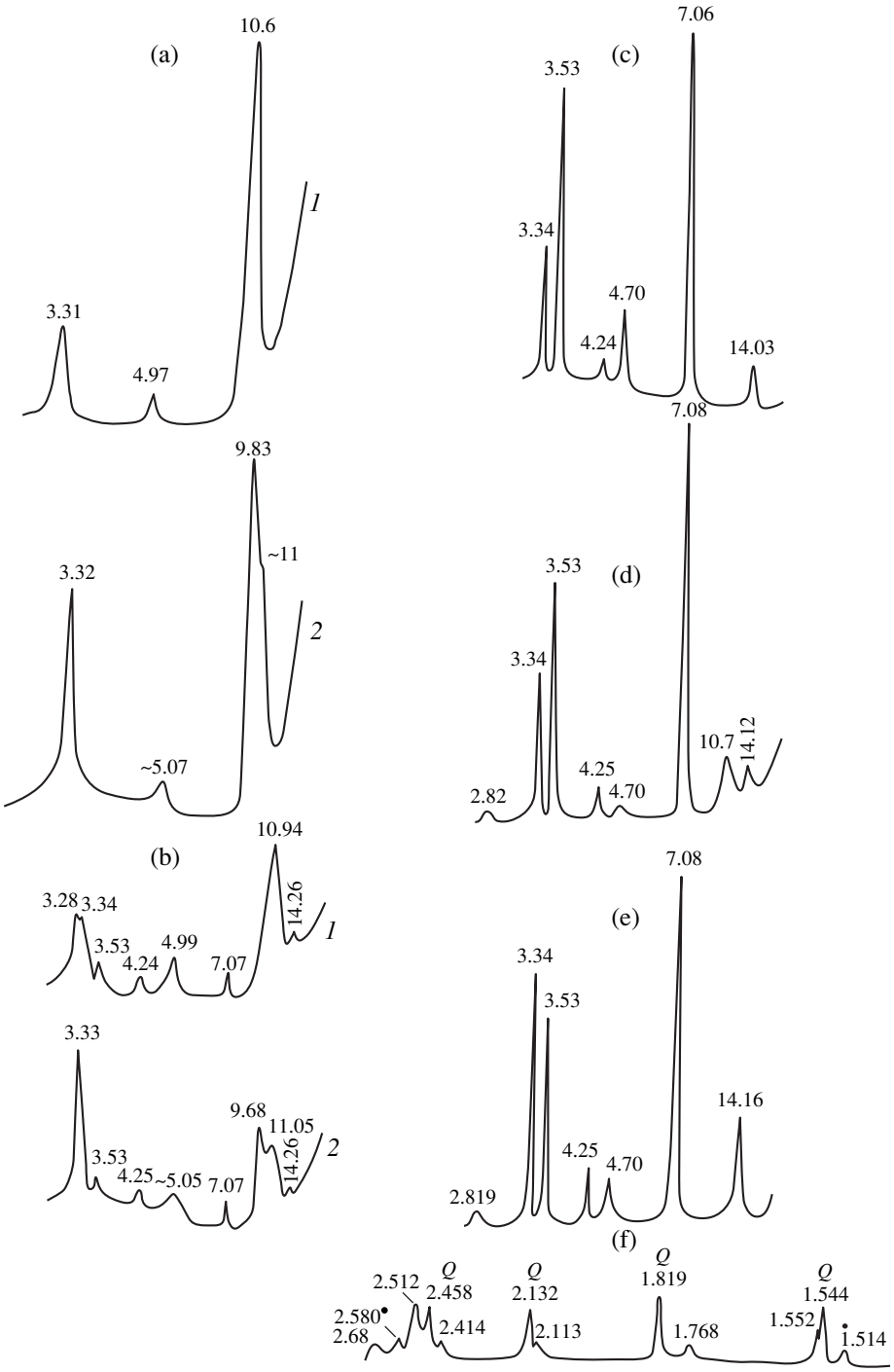

Fig. 5. Diffractograms of oriented samples. (a, b) Glauconite globules in the (*1*) air-dry and (*2*) ethylene glycol-saturated states: (a) Sample 556), (b) sample 578/8e; (c–e) chlorite in the natural state: (c) sample 578/3e, (d) sample 578/4b, (e) sample 578/3a; (f) diffractogram of unoriented sample 578/3a. Dots mark reflections of the micaceous mineral. (Q) Quartz.

sections (samples 578/3a, 578/4b). Sandy–silty rocks were used to analyze the following materials: (1) green, brownish green, and brownish (samples 556a, 566c, 578/4) and greenish brown (sample 581b) globules; (2) chlorite patches in brownish grains (sample 578/4); (3) brownish clayey strata (sample 578/4); (4) chlorite segregations in the clayey strata (sample 578/4); and (5) pellets represented by colorless (sample 556a), green (samples 578/2, 578/4), and brown (samples 578/3e, 578/2, 581b, 566c, 578/4) varieties.

The application of a Camscan scanning electron microscope equipped with microprobe analyzer made it

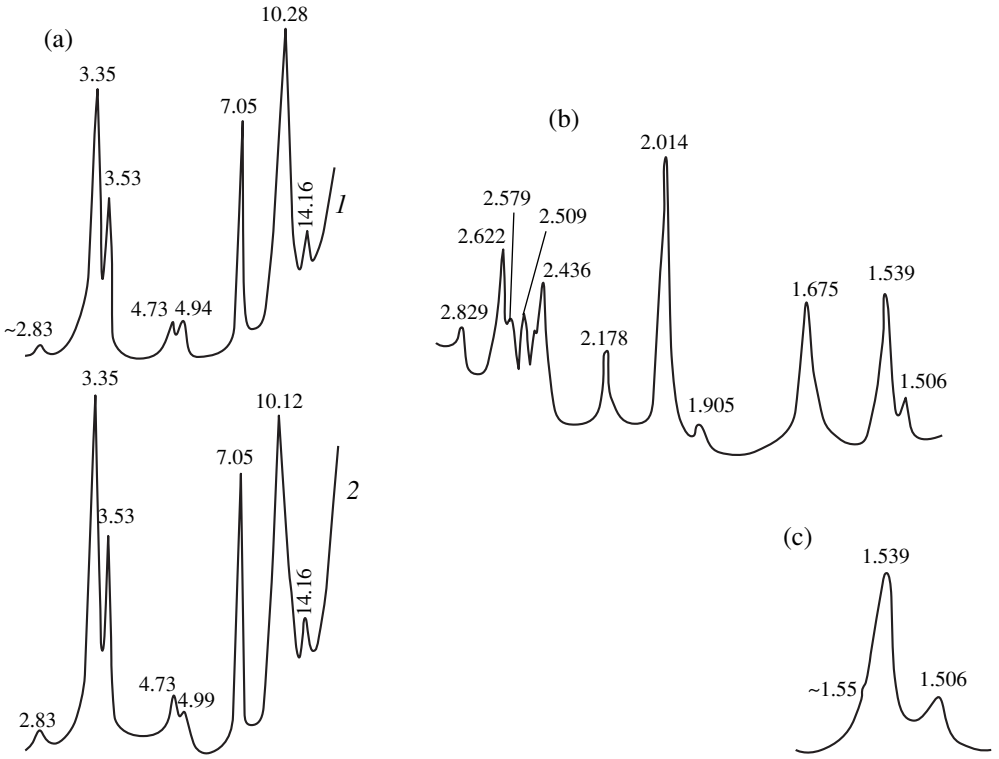

Fig. 6. Diffractograms of (a) oriented and (b) unoriented samples of brown pellets (sample 566/3). (c) 060 region in the discrete regime.

possible to carry out the qualitative and quantitative analysis of minerals or their assemblages in mudstones (samples 578/a, 578/4b) and silty sandstones (samples 578/4, 578/3e, 566/3).

In samples 556 and 566/2, the microprobe analysis was supplemented with the complete silicate analysis.

Chemical composition of globular glauconite. As is evident from Table 2, green globules taken from different levels of the subformation show a wide range of contents of Al_2O_3 (14.74–22.74%) and Fe_2O_3 (7.84–15.42%). As will be shown below, such variations can occur even in a single sample (monofraction and polished section). The variation is smaller in the case of K_2O (7.05–8.56%) and MgO (1.94–2.61%), except for sample 578/9b (MgO 4.81%), probably, owing to the chlorite admixture recorded in the X-ray spectra.

In order to compare the accuracy of data obtained by different methods, Table 2 presents not only the microprobe analyses, but also the complete silicate analyses (including the determination of water) of samples 556 and 566/2. It is evident that the microprobe analysis yields slightly higher contents of SiO_2 and K_2O (Table 2, analyses 1, 2, 9, 10).

When calculating crystallochemical formulas of minerals (Table 3) based on complete and incomplete silicate analyses, we assumed that the anionic framework of $(O_{10}(OH)_2)^{-22}$ is constant. Table 3 shows that octahedral sites of 2 : 1 layers of minerals are dominated by Al cations (0.86–1.35 f.u.). The content of total Fe (hereafter, Fe^{3+}) cations varies from 0.40 to 0.85 f.u.; Mg cations, from 0.20 to 0.50 f.u.; and the interlayer K cations, from 0.64 to 0.76 f.u.

Thus, crystallochemical features described above indicate that the studied minerals correspond to Al-glauconites. In terms of the Fe index ($n = Fe^{3+}/Fe^{3+} + Al$), they make up a continuous isomorphous series ($n = 0.23–0.49$). Among them, the Al-rich varieties ($Al_{VI} = 1.21–1.35$ f.u., $Fe^{3+} = 0.40–0.50$ f.u.) make up samples 578/2, 578/3e, and 578/8e ($n = 0.23–0.31$). The Fe-rich varieties ($Al_{VI} = 0.93$ and 0.86 f.u.; $Fe^{3+} = 0.85$ and 0.81 f.u.) compose samples 566b and 556 ($n = 0.48$ and 0.49, respectively).

Chemical composition of brownish grains. As was mentioned above, green globules in the studied polished sections are supplemented with brownish green and brownish varieties (samples 556a, 578/2, 578/4, 566c). Their compositions are slightly different from that of Al-glauconite in green globules from the same polished section. Table 4 shows compositional variations of micaceous minerals in the green, brownish green, and brownish grains (sample 578/4). It is evident that the Al_2O_3 content increases from 16.99% in the green variety to 26.17% in the brownish variety, while the Fe_2O_3 content decreases from 12.89 to 6.60%. A similar variation is also recorded in globules of different colors (samples 556a, 566c). This trend is also sup-

ported by the semiquantitative analysis of the brownish (Fig. 2c, analyses 46–51) and green globules.

The averaged crystallochemical formula of minerals in brownish globules (sample 578/4) is as follows:

$$K_{0.65}Na_{0.004}Ca_{0.04}(Al_{1.49}Fe^{3+}_{0.33}Mg_{0.20})_{2.02}[Si_{3.43}Al_{0.57}]O_{10}(OH)_2.$$

This formula shows that, relative to Al-glauconite, minerals in the brownish grains from green globules (Table 3, sample 578/4) are characterized by higher contents of octahedral and tetrahedral Al cations and lower

Table 2. Chemical composition of glauconite globules (wt %)

Analysis no.	Sample no.	Grain size, mm	Grain density, g/cm^3	Oxides								
				SiO_2	Al_2O_3	Fe_2O_3	FeO	MgO	CaO	Na_2O	K_2O	total
Ochchugui-Sololi River												
1	556	0.315–0.16	2.7–2.75	50.05	15.40	12.58	2.47	2.35	0.93	0.13	7.25	91.16
2	556	0.315–0.16	2.7–2.75	52.41	15.22	14.50		2.58	0.28	absent	8.14	93.15
3	556a	0.2–0.16	–	52.86	18.03	12.12		2.60	0.43	0.01	8.18	94.33
Debengda River												
4	578/2	0.16–0.1	–	52.91	21.84	8.89		2.19	0.49	0.01	7.88	94.21
5	578/3e	0.16–0.1	–	52.02	22.74	7.84		2.12	0.44	0.11	8.13	93.60
6	578/4	0.315–0.16	–	52.11	16.99	12.89		2.52	0.37	0.04	8.11	93.07
7	566/1	0.315–0.16	2.7–2.8	52.35	18.57	9.36	2.81	2.33	0.37	0.06	7.96	94.21
8	566c	0.16–0.1	–	53.10	17.99	11.48		2.54	0.43	0.03	7.98	93.56
9	566/2	0.315–0.16	2.65–2.75	50.54	17.04	11.43	2.23	2.32	0.12	0.16	7.05	90.89
10	566/2	0.315–0.16	2.65–2.75	52.19	17.28	13.04		2.20	0.03	absent	8.14	92.91
11	566b	0.4–0.2	–	52.35	14.75	15.42		2.61	0.39	0.01	8.24	93.80
12	578/8e	0.16–0.1	–	52.05	19.23	10.45		1.94	0.23	0.01	7.41	91.36
13	578/9b	0.2–0.1	–	53.04	14.74	11.39		4.81	0.19	0.05	8.56	92.85

Note: In samples 556 (analysis 1) and 566/2 (analysis 9), the H_2O^+ content is 5.34 and 3.00%, respectively; the H_2O^- content is 7.52 and 1.37%, respectively. Hereafter, each microprobe analysis is an average based on three analyses.

Table 3. Crystallochemical formulas of minerals of the glauconite series (f.u.)

Formula no.	Sample no.	Grain size, mm	Grain density, g/cm^3	Cations									*n*
				tetrahedral		octahedral				interlayer			
				Si	Al	Al	Fe^{3+}	Fe^{2+}	Mg	Ca	Na	K	
1	556	0.315–0.16	2.7–2.75	3.62	0.38	0.93	0.57	0.28	0.25	0.07	0.02	0.67	0.48
2	556a	0.2–0.16	–	3.61	0.39	1.07	0.62		0.27	0.03	0.001	0.71	0.37
3	578/2	0.16–0.1	–	3.56	0.44	1.30	0.45		0.22	0.04	0.001	0.68	0.26
4	578/3e	0.16–0.1	–	3.53	0.47	1.35	0.40		0.26	0.03	0.01	0.70	0.23
5	578/4	0.315–0.16	–	3.62	0.38	1.02	0.67		0.26	0.03	0.005	0.72	0.40
6	566/1	0.315–0.16	2.7–2.8	3.60	0.40	1.10	0.52	0.15	0.24	0.03	0.008	0.70	0.38
7	566c	0.16–0.1	–	3.63	0.37	1.09	0.60		0.26	0.03	0.004	0.71	0.36
8	566/2	0.315–0.16	2.65–2.75	3.61	0.39	1.04	0.61	0.13	0.25	0.01	0.02	0.64	0.42
9	566b	0.4–0.2	–	3.65	0.35	0.86	0.81		0.27	0.03	0.001	0.73	0.49
10	578/8e	0.16–0.1	–	3.63	0.37	1.21	0.55		0.20	0.02	0.001	0.66	0.31
11	578/9b	0.2–0.1	–	3.70	0.30	0.91	0.60		0.50	0.01	0.007	0.76	0.40

Note: (–) No data.

Table 4. Chemical composition of globular micaceous minerals of different colors in sample 578/4 (wt %)

Oxides	1	2	3	4	5	6	Average content	7	8	Average content	9	10	11	Average content	12
SiO_2	52.90	52.56	51.14	52.61	51.15	52.28	52.10	52.11	52.52	52.32	52.51	50.12	51.50	51.38	52.65
TiO_2	0.02	0.01	0.05	0.01	0.03	0.03	0.03	0.07	0.04	0.05	0.02	0.04	0.07	0.06	0.07
Al_2O_3	15.78	15.16	18.47	20.74	13.34	18.45	16.99	22.72	22.49	22.61	25.51	26.14	26.85	26.17	21.09
Fe_2O_3	14.29	13.61	12.29	9.69	15.87	11.59	12.89	9.54	8.75	9.15	5.38	7.93	6.50	6.60	11.30
MgO	2.36	2.48	2.58	2.22	3.03	2.44	2.52	2.20	2.12	2.16	1.86	2.64	1.65	2.05	2.29
CaO	0.34	0.33	0.42	0.32	0.59	0.24	0.37	0.49	0.46	0.47	0.54	0.51	0.51	0.52	0.50
Na_2O	0.02	absent	0.18	0.04	0.02	absent	0.06	absent	absent	absent	0.01	0.03	0.06	0.03	absent
K_2O	7.96	7.99	8.05	8.04	8.21	8.39	8.11	8.14	8.23	8.17	7.52	7.37	8.00	7.63	7.94
Total	93.67	92.14	93.18	93.70	92.24	93.42	93.07	95.27	94.64	94.95	93.35	94.78	94.96	94.66	95.84

Note: (1–12) Sample numbers. Globule color: (1–6) green, (7, 8) brownish green, (9–12) brownish.

contents of octahedral Fe cations. With respect to composition, such brownish grains can be referred to as Fe-illite.

The chlorite-bearing brown globules can be composed of Fe-illite (Table 4, analysis 12) or chlorite and illite. The latter (mixed) composition will be described below. The presence of both compositional types within a single grain is also confirmed by the semiquantitative microprobe analysis (Fig. 2b).

Chemical composition of chlorite. Microprobe analyses of brownish globules and clayey strata in glauconite-bearing rocks (sample 578/4) revealed that chlorites in both materials are virtually similar. This is indicated by similar average contents of the following major oxides (%): SiO_2 25.88, 26.12; Al_2O_3 23.25, 23.46; FeO 33.64, 33.94; and MgO 6.85, 6.70 (Table 5, analyses 3–6). The crystallochemical formula calculated for the globular chlorite fits the Fe^{2+}–Mg composition (Table 6, formula 1).

Chlorite developed as spherulitic aggregates in clayey strata of siltstones (sample 578/3e) is generally similar to its counterpart developed as interlayers in mudstones (samples 578/3a, 578/4b) (Table 5, analyses 7–15).Their crystallochemical formulas also fit the Fe^{2+}–Mg composition. Among them, sample 578/4b is marked by the highest Fe content (Table 6, formulas 2–4).

The semiquantitative chemical analysis of chlorites (30 analyses) in globules and interstitial cement (sample 578/4) and clayey strata (sample 578/3e) also yielded similar compositions. Figure 7 presents three representative analyses.

The greenish gray globules (sample 581b) are composed of chlorite with a minor admixture of mica, as suggested by the presence of a small amount of K cations (K_2O 1.39%) (Table 5, analyses 1, 2). Calculation of the crystallochemical formula without the consideration of the micaceous phase suggested that the globular chlorite in sample 581b (Table 6) also fits the Fe^{2+}–Mg composition. However, this chlorite variety is marked by the highest Mg content relative to the varieties described above.

Chemical composition of mica–chlorite blends in globules and clayey rocks. The brownish globules and

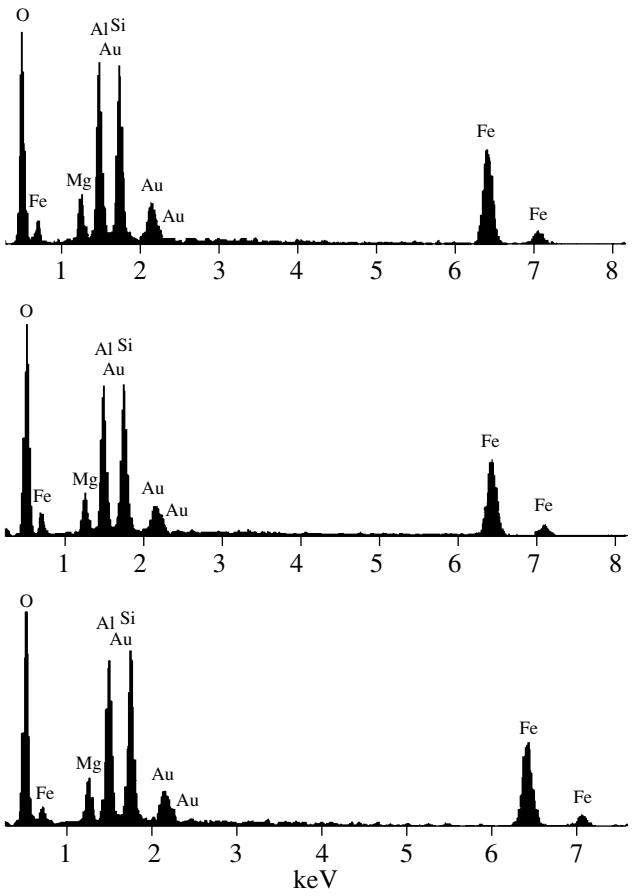

Fig. 7. X-ray spectra of chlorites in the brownish globule (analysis 60a) and pore cement (analysis 63) of sample 578/4, as well as in the clayey stratum of sample 578/3e (analysis 7). Camscan SEM images (semiquantitative analysis).

Table 5. Chemical composition of chlorite in globules and rocks (wt %)

Oxides	1	2	Total	3	4	Total	5	6	Total	7
	Globules						Rock			
SiO_2	28.22	29.15	28.68	26.07	25.69	25.88	26.10	26.14	26.12	27.67
TiO_2	0.01	0.01	0.01	0.02	0.04	0.03	0.04	0.01	0.07	0.12
Al_2O_3	21.23	20.05	20.64	23.53	22.95	23.25	23.83	23.08	23.46	24.02
FeO	31.12	29.49	30.31	33.64	33.64	33.64	34.03	33.84	33.94	30.24
MgO	9.06	7.96	8.51	6.35	6.85	6.85	6.81	6.58	6.70	7.01
CaO	0.21	0.16	0.19	0.07	0.10	0.08	0.07	0.09	0.08	0.08
K_2O	1.48	1.30	1.39	0.09	0.15	0.12	0.09	0.17	0.13	0.14
Total	91.33	88.12	89.73	90.27	89.42	89.85	90.97	89.91	90.43	89.28
Oxides	Rock									
	8	9	10	11	12	Total	13	14	Total	15
SiO_2	27.45	27.47	27.14	27.31	27.39	27.41	27.43	26.48	26.96	24.82
TiO_2	0.03	0.08	0.09	absent	absent	0.08	0.06	0.08	0.07	0.36
Al_2O_3	24.01	24.24	23.62	23.96	23.84	23.94	20.80	21.26	21.03	18.84
FeO	31.27	29.44	31.88	31.24	30.96	30.83	31.08	30.40	30.74	37.99
MgO	7.19	6.91	7.27	7.17	7.09	7.11	5.91	5.91	5.91	5.29
CaO	0.07	0.11	0.06	0.06	0.09	0.09	0.14	0.19	0.16	0.11
K_2O	0.14	0.41	0.24	0.10	0.22	0.20	0.17	0.14	0.16	0.22
Total	90.16	88.66	90.3	89.84	89.59	89.66	85.59	84.46	85.09	87.63

Note: (1–15) Analysis numbers. Chlorite globules from sample 581b (analyses 1, 2); chlorite sectors in brownish globules from sample 578/4 (analyses 3, 4); the same in clayey strata from sample 578/4 (analyses 5, 6) and sample 578/3e (analyses 7–12); chlorite in mudstones from sample 578/3a (analyses 13, 14) and sample 578/3b (analysis 15).

Table 6. Crystallochemical formulas of chlorites (f.u.)

Formula no.	Sample no.	Cations					
		tetrahedral		octahedral			
		Si	Al	Al	Fe^{2+}	Mg	total
1	578/4	2.75	1.25	1.68	3.00	1.09	5.77
2	578/3e	2.88	1.12	1.84	2.71	1.11	5.66
3	578/3a	3.00	1.00	1.76	2.87	0.98	5.61
4	578/4b	2.84	1.16	1.33	3.67	0.90	5.90
5	566c	3.13	0.87	1.54	2.93	1.19	5.66
6	581b	3.03	0.97	1.19	3.14	1.58	5.91
7	581b	3.25	0.75	1.75	2.39	1.37	5.51

Note: Formulas were calculated for chlorites from the brownish and greenish gray globules (analyses 1, 6), the clayey strata (2), mudstones (3, 4), and gray pellets (5, 7).

clayey strata, which are replaced by large chlorite flakes (sample 578/4), mainly represent Fe-illite–chlorite blends, i.e., intermediate compositions (Table 7, analyses 1, 2, 5). In particular, they are characterized by low contents of SiO_2 and K_2O. At the same time, contents of FeO and MgO are higher. Globules are dominated by the micaceous phase, while the clayey rock is mainly composed of chlorite.

Judging from the semiquantitative analysis data, in one of the clayey strata in sample 578/3e (Fig. 2d) almost completely replaced by chlorite (analysis 10) and calcite (analysis 9), the retained clayey component

Table 7. Chemical composition of mica–chlorite blends in globules and brownish clayey rocks (wt %)

Oxides	1	2	3	4	5
	Globules		Rock		
SiO_2	43.61	42.23	45.35	41.47	37.37
TiO_2	0.16	0.18	0.30	0.26	0.09
Al_2O_3	24.19	22.85	22.81	21.86	24.04
FeO	16.05	14.84	14.66	18.44	21.83
MgO	3.31	3.67	3.51	3.83	5.81
CaO	0.38	0.34	0.50	0.03	0.25
Na_2O	0.01	0.01	0.03	0.28	0.01
K_2O	5.35	5.07	4.00	3.70	2.43
Total	93.02	89.23	91.16	89.87	92.17

Note: (1–5) Sample numbers. (1, 2) Brownish globules and (5) brownish clayey interlayer from sample 578/4; (3, 4) mudstones from sample 578/3a.

Table 8. Chemical composition of pellets of different colors (wt %)

Oxides	1	2	3	4	5	6	7	8	9	10	11	12	13
	$Al_2O_3 > FeO$							$FeO > Al_2O_3$					
SiO_2	45.57	53.41	52.01	52.85	50.87	48.94	42.65	34.11	38.60	32.85	32.79	36.56	35.84
TiO_2	0.03	0.09	0.02	absent	0.31	0.14	0.18	0.04	0.04	1.90	0.57	2.13	1.64
Al_2O_3	32.97	17.35	21.65	23.44	25.97	26.40	24.98	20.01	19.08	18.21	20.03	19.42	19.89
Fe_2O_3	5.59	13.36	9.65	4.92	4.01	6.69	11.23	25.57	22.60	25.29	23.81	24.89	25.72
MgO	1.03	2.65	2.01	1.84	2.82	3.16	3.82	8.05	7.11	7.95	6.39	4.91	6.40
CaO	0.01	0.46	0.34	0.66	0.52	0.51	0.38	0.61	0.60	0.40	0.31	0.27	0.20
Na_2O	0.17	0.03	absent	absent	0.08	0.26	0.07	0.50	0.36	0.47	0.17	0.01	absent
K_2O	9.98	8.08	7.87	7.25	7.95	5.94	4.87	1.11	1.48	1.53	1.68	5.86	5.95
Total	95.35	95.43	93.56	90.96	92.53	91.81	88.18	90.00	89.87	88.60	85.75	94.05	95.67

Note: (1–13) Analysis numbers. (1) Colorless (sample 556a); (2, 3) green: (2) sample 578/2, (3) sample 578/4; (4–13) brown: (4–6) sample 578/e, (7) sample 578/2, (8–10) sample 581b, (11) sample 566c, (12, 13) sample 578/4. In analyses 1–5, Fe is mainly present in the trivalent form; in analyses 8–13, in the bivalent form. In analyses 6 and 7, the contents of the bivalent and trivalent forms are governed by the ratio of micaceous and chloritic components.

Table 9. Crystallochemical formulas of lamellar micaceous minerals (Fe-muscovite, Al-glauconite, and Fe-illite)

Formula no.	Sample no.	Cations							
		tetrahedral		octahedral			interlayer		
		Si	Al	Al	Fe^{3+}	Mg	Ca	Na	K
1	556a	3.06	0.94	1.67	0.28	0.10	0.008	0.02	0.85
2	578/2	3.62	0.38	1.01	0.69	0.27	0.03	0.003	0.69
3	578/4	3.55	0.45	1.28	0.49	0.20	absent	0.02	0.68
4	578/3e	3.45	0.55	1.53	0.20	0.28	0.08	0.03	0.68

Note: Colorless (sample 556a), green (samples 578/2, 578/4), and brown (sample 578/3e) varieties were analyzed.

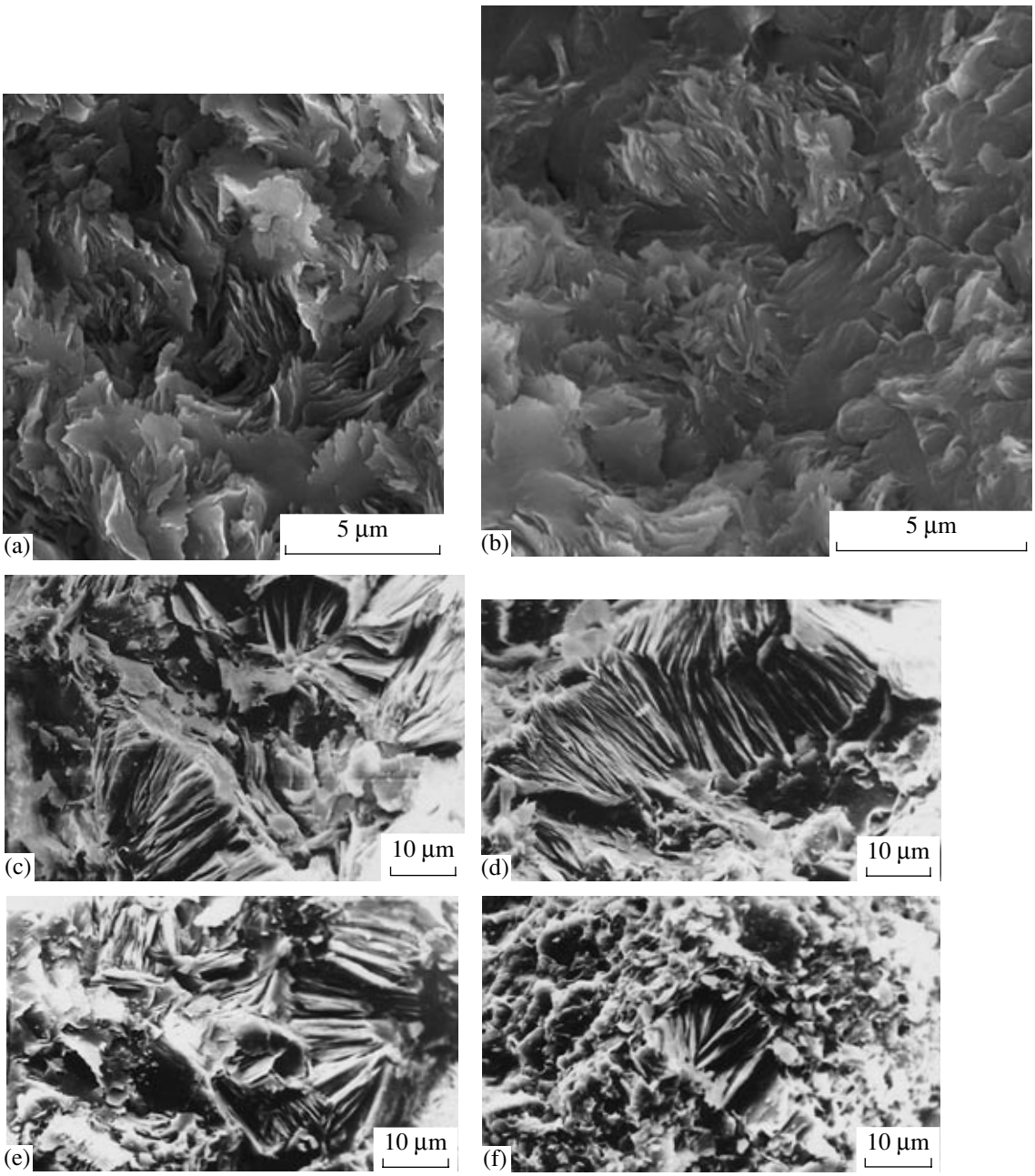

Fig. 8. Microtextures of glauconite and chlorite in samples 578/4 (a, b) and 578/3e (c–f). (a) Glauconite; (b) chlorite crystallites among glauconite flakes (right-hand lower corner), globule chips, Camscan SEM image, (c–f) microtexture of chlorite in clayey strata, Stereoscan-600 SEM images.

is composed of a blend of micaceous minerals, chlorite, and quartz (analysis 11).

In two sectors of mudstone (sample 578/3a), one can see the mixing of chlorite and mica (Table 7, analyses 3, 4). This type of blend occasionally includes quartz, as suggested by the qualitative microprobe data (samples 578/3a, 578/4b).

Chemical composition of pellets of various colors. The **colorless pellet** found in sample 556a (Table 8, analysis 1) is enriched in Al_2O_3 (32.97%) and K_2O (9.98%), but depleted in the total Fe (5.59%) and MgO (1.03%). The composition of this variety fits Fe-muscovite, as suggested by its crystallochemical formula (Table 9, formula 1). A similar ratio of oxides is observed in semiquantitative analyses of the colorless pellets from samples 578/3e and 566/3.

Green pellets (samples 578/2, 578/4) characterized by the predominance of Al cations (17.35 and 21.65%, respectively) over the total Fe content (13.36 and 9.65%, respectively) can be referred to as Al-glauconite

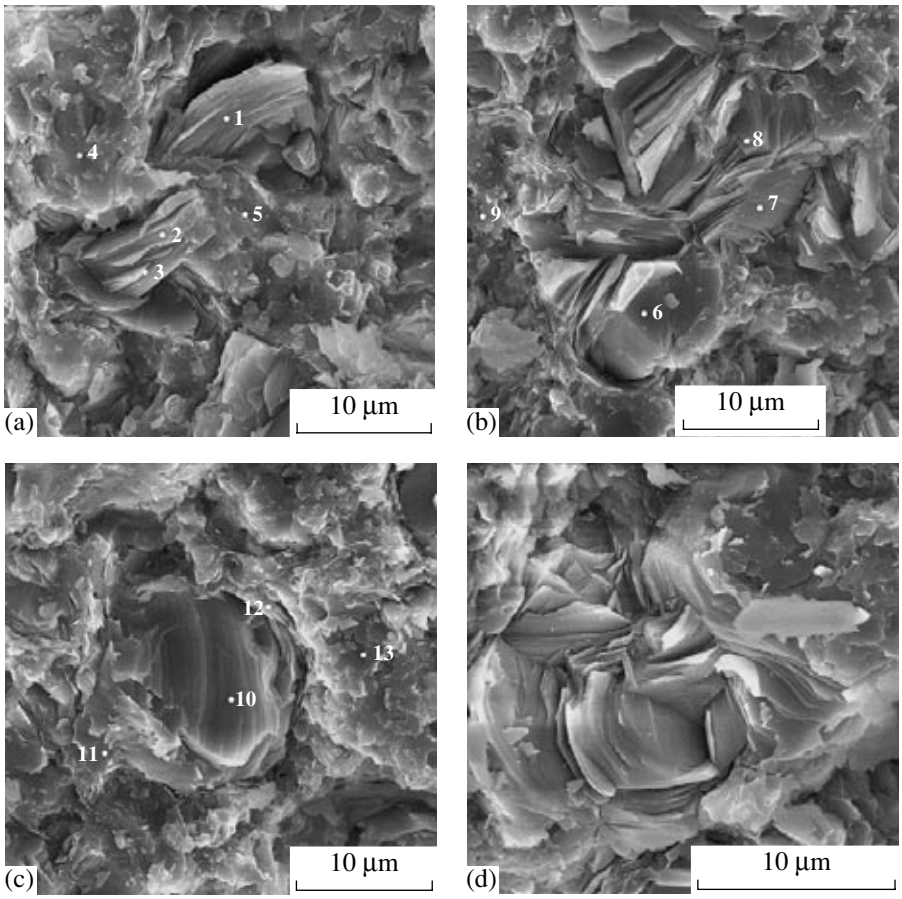

Fig. 9. Microtexture of mudstone (sample 578/4b), Camscan SEM images (qualitative analysis). (a–c) Large chlorite monocrystals (analyses 1, 3, 6–8, 10, 12) that often make up packages among the finer flaky matrix composed of chlorite with an admixture of quartz and other minerals (analyses 2, 4, 9, 11, 13); (d) concentric-layered chlorite crystallites.

with different Fe contents (Table 8, analyses 2, 3). Their crystallochemical formulas are given in Table 9.

Brown pellets (samples 578/3e, 578/2, 581b, 566c, 578/4) have different compositions (Table 8, analyses 4–13). In some varieties, Al_2O_3 prevails over the total Fe (Table 8, analyses 4–7), while the relationship is opposite in other varieties (Table 8, analyses 8–13). At the same time, both groups differ in the K_2O content.

The brown pellets (Table 8, analyses 4, 5) with high contents of Al_2O_3 (23.44 and 25.97%) and K_2O (7.25 and 7.95%) and a small amount of the total Fe (4.92 and 4.01%) can be referred to as Fe-illite. This is also suggested by the crystallochemical formula (Table 9) calculated for one brown pellet (sample 578/3e).

The K-depleted and Al-enriched brown pellets (Table 8, analyses 6, 7) have higher contents of FeO (6.69 and 11.23%) and MgO (3.16 and 3.82%). Hence, such pellets can be two-phase minerals, in which Fe-illite is the major component, whereas Fe^{2+}–Mg-chlorite is subordinate. The latter component is slightly higher in sample 578/2 (Table 8, analysis 7).

The brown pellets with Fe cations dominating over Al cations (Table 8, analyses 8–13) are enriched in MgO (6.39–8.05%) and occasional TiO_2 (0.57–2.13%). In terms of the K_2O content, such pellets can be divided into two groups. The K-poor variety (K_2O 1.11–1.68%) is composed of Fe^{2+}–Mg-chlorite with an admixture of the micaceous phase (Table 8, analyses 8–11). This is evident from crystallochemical formulas of pelletal chlorites from samples 566c and 581b (Table 6) based on the averaged analyses and the consideration of the contribution of micaceous phases.

The K-enriched varieties (K_2O 5.86 and 5.95%) can be a complex compound of mineral phases mainly dominated by the terrigenous biotite (Table 8, analyses 12, 13). The subordinate component can be represented by different proportions of Fe-illite and/or chlorite (sample 578/4).

The statistical semiquantitative chemical analysis of 35 brown pellets in the polished section of sample 566/3 revealed the following fact. In terms of the ratio of oxides, three pellets are compositionally similar to Fe-illite, while the remaining pellets can be referred to as minerals of the biotite–phlogopite series. Among

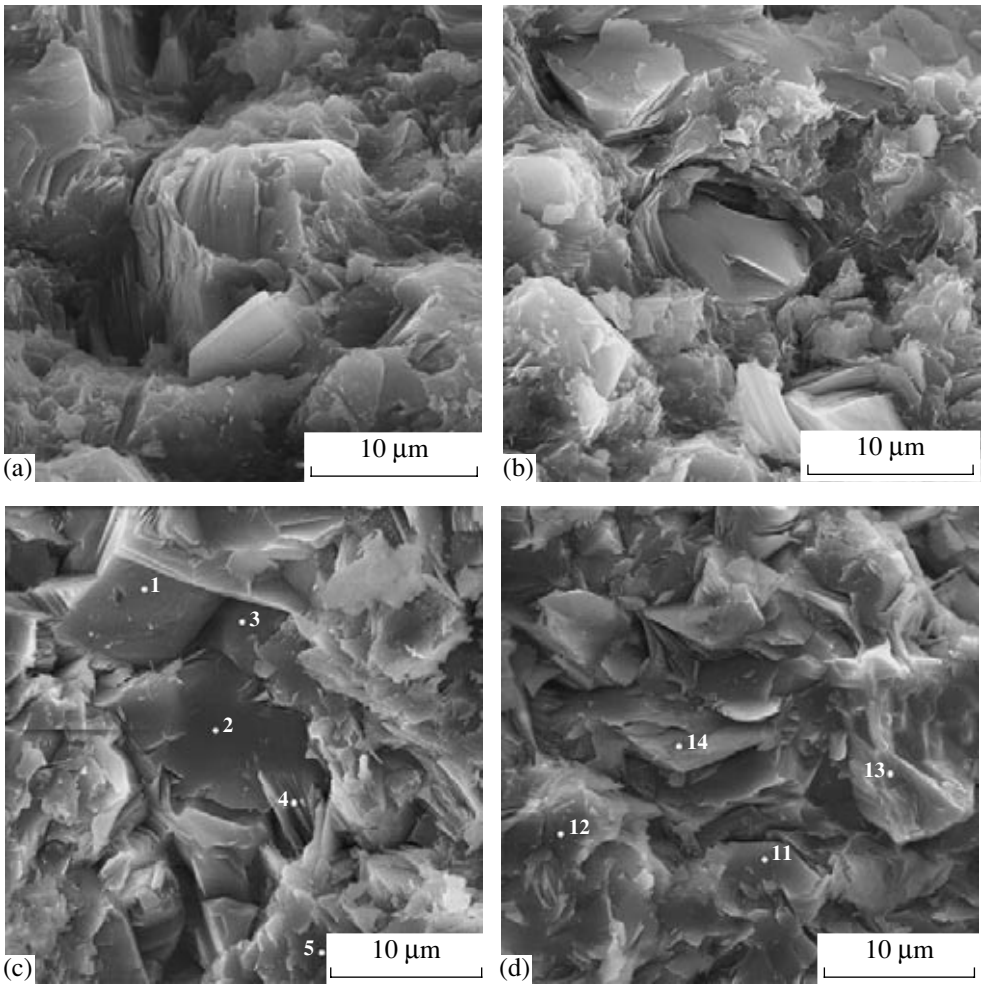

Fig. 10. Microtexture of mudstones. Camscan SEM images (qualitative analysis). (a, b) Sample 578/4b, chlorite crystallites of different shapes; (c, d) sample 578/3a, chlorite crystallites (analyses 4, 5, 11–14) among quartz grains (analyses 1–3).

them, the K-depleted varieties can be chloritized phases. These results are also supported by the X-ray data, which indicate that the major phase in the brown pellets from sample 566/3 correspond to biotite. The secondary components are represented by micaceous minerals and chlorite (Fig. 6).

MICROTEXTURE OF SAMPLES

Using Stereoscan-600 and Camscan scanning electron microscopes equipped with microprobe devices, we studied the following materials (Fig. 3): (1) glauconite-bearing sandy–silty rocks (samples 578/3e, 578/4, 566/1), in which globules and crystalline chlorite in the globules, cement, and clayey strata were analyzed; (2) mudstones (samples 578/3a, 578/4b); and (3) glauconite globules differently replaced by hematite (samples 566b, 578/8b).

Glauconite globules are commonly characterized by intricate-flaky microtexture with the crystallite size ranging from 1–2 to 4–5 μm (Fig. 8a). Like the optical microscopic study of thin sections, the scanning electron microscopic examination of numerous green globules revealed that chlorite is rather scarce in the globules. Moreover, chlorite has a more massive microtexture relative to glauconite (Fig. 8b).

In clayey strata of glauconite-bearing rocks (samples 578/3e, 578/4), chlorite occurs as large (from 3–6 to 10–20 μm) pelletal, hexagonal and/or irregular crystallites with rectilinear or curved faces (Figs. 8c–8f). They often make up isolated or stacked packages among the smaller crystallites of clay minerals. Based on X-ray and microprobe data, the clay minerals are represented by micaceous minerals, chlorite, and quartz. Their proportions are highly variable at different observation points.

In mudstone of sample 578/4b, the groundmass is composed of a dense cluster of equant flakes (from <0.1 to 4 μm in size), which include numerous patches of larger (up to 10–15 μm) chlorite crystallites (Fig. 9).

Investigation of mudstone in sample 578/4b with the help of a Camscan SEM revealed the following features

(Figs. 9a–9c). Based on the distribution of FeO, MgO, SiO_2, and Al_2O_3 in the groundmass, the flakes are composed of chlorite or chlorite–quartz blend (analyses 4, 9, 11, 13). Minor concentrations of K_2O and TiO_2 suggest that the admixture is represented by micaceous minerals and/or anatase. The flake groundmass includes large (up to 8–15 μm) crystallites of equant, pelletal, and pseudohexagonal chlorite (Fig. 9a–9c, analyses 1–3, 6–8, 10, 12). Rectilinear and/or curved chlorite crystallites often make up concentric-conchoidal aggregates resembling buds, rosettes, and helmets (Figs. 9d, 10a, 10b). Large crystallites also occur as isolated dense aggregates (Fig. 9c) and/or clusters that can be subparallel or inclined relative to each other (Figs. 9a, 9b). In thin sections, one can see that the diverse clusters of large crystallites make up a granular mass among the fine-grained mica–chlorite matrix.

In mudstone from sample 578/3a, chlorite crystallites, which are similar to those described above in terms of shape and size (analyses 4, 5, 11–14), corrode and often make up a rim around the numerous quartz grains, resulting in the interweaving of flakes and their aggregates. In Figs. 10c and 10d, one can see the development of chlorite crystallites around quartz grains (analyses 1–3). Some crystallites penetrate the quartz grains. The concentric-zonal structure of crystallites, a typical feature of mudstones in sample 578/4b, is very rare in sample 578/3a.

DISCUSSION

Based on the detailed investigation of data on sections of the lower subformation of the Arymas Formation, let us examine phases of the formation and transformation of dioctahedral and trioctahedral phyllosilicates (biotite, glauconite, Fe-illite, and Fe^{2+}–Mg-chlorite) at different stages of lithogenesis.

Diagenesis

Globular glauconite. As was shown above, the studied samples are represented by hydromicas with an ordering trend in the alternation of mica and smectite layers ($S > 1$). In terms of composition, they correspond to Al-glauconites with different Fe contents (Tables 1–3; Figs. 5a, 5b). The globule composition is variable not only in different samples, but also in different grains within a single sample (Table 4, analyses 1–6), testifying to the chemical heterogeneity of the globular Al-glauconite.

Previously, we noted the chemical heterogeneity of minerals of the glauconite–illite series (from Al-glauconite to glauconite) in different grains within a single sample from the Middle Riphean Debengda Formation of the Olenek High and the Vendian–Cambrian Khmel'nitsk Formation of Podolia (Ivanovskaya, 1994; Ivanovskaya et al., 1999).

According to (Shutov et al., 1975; Shutov, 1984; Drits and Kossovskaya, 1986; Tsipurskii et al., 1992; Ivanovskaya et al., 1999), glauconite grains of different lithologies and ages are characterized by compositional heterogeneity at the macroscopic level (in globules within a single sample) and the microscopic level (inside the globule within a single crystallite).

Intricate diffraction features of glauconite hydromicas ($S > 1$) are typical of all studied samples. Such features have been rarely mentioned in the available literature. For example, they were not noted in the voluminous collection of glauconite grains of different ages and locations studied by Nikolaeva (1977). Drits et al. (1993) investigated a part of this collection. However, they presented only theoretical versions of diffraction curves for the glauconite–smectite series with $S = 1$, 2, and 3.

In this connection, we should note that Thompson and Hower (1975) compared experimental and calculated curves for six (among 19) different-age glauconite samples and concluded that glauconite and smectite layers always show ordered alternation if the content of smectite layers is <30% (at 10–25%, $S = 1$; at 10–15%, $S = 3$). The alternation is unordered ($S = 0$) only if the content is >30% (Thompson and Hower, 1975).

The representative samples collected by Ivanovskaya contains not only samples from the Arymas Formation, but also other hydromicas of the glauconite composition (with $S > 1$) from Precambrian, Lower Cambrian, and Lower Cretaceous rocks (Ivanovskaya et al., 1989, 1991; Ivanovskaya, 1996; Geptner and Ivanovskaya, 2000; Ivanovskaya and Geptner, 2004).

It is worth mentioning that samples with the ordering trend are characterized by both "rejuvenated" and stratigraphically significant isotope ages (Semikhatov et al., 1987; Gorokhov et al., 1997; Zaitseva et al., 2005). In addition, both usual glauconite hydromicas ($S = 0$) and hydromicas with the ordering trend ($S \geq 1$) were noted in a single section of the Middle Riphean Totta Formation (Aim River) at close stratigraphic levels (Ivanovskaya et al., 1989).

Pelletal glauconite. The formation of pelletal glauconite after the terrigenous biotite in diagenesis zone has been discussed and proved on the basis of microscopic investigation by many researchers (Galliher, 1935; Fenoshina, 1961; Murav'ev, 1962; Kopeliovich, 1965; Millot, 1965; Triplehorn, 1966; and others). This fact has also been supported by scanning electron microscopic, X-ray, chemical, and Mössbauer analysis data (Ivanovskaya et al., 1993).

Scheme of the rearrangement of trioctahedral biotite into dioctahedral glauconite is presented in (Ivanovskaya et al., 2003). Here, let us only note that the rearrangement takes place according to the solid-phase mechanism with the application of the major structural elements of the mica matrix.

Table 10. Chemical composition of micaceous minerals, chlorites, and their blends in globules and rocks (wt %)

Oxides	Globules					Rock					
	A			B		I			II		
	1	2	3	4	5	6	7	8	9	10	11
SiO_2	52.65	42.23	25.69	43.61	26.07	37.71	26.10	26.14	45.35	41.47	26.96
TiO_2	0.07	0.18	0.04	0.16	0.07	0.09	0.04	0.01	0.30	0.26	0.07
Al_2O_3	21.09	22.85	22.95	24.19	23.53	24.04	23.83	23.08	22.81	21.86	21.03
FeO	11.30	14.84	33.64	16.05	33.64	21.83	34.03	33.84	14.66	18.44	30.74
MgO	2.29	3.67	6.85	3.31	6.85	5.81	6.81	6.58	3.51	3.83	5.91
CaO	0.50	0.38	0.10	0.34	0.07	0.25	0.07	0.09	0.50	0.03	0.16
Na_2O	absent	0.01	absent	0.01	absent	0.01	absent	absent	0.03	0.28	absent
K_2O	7.94	5.07	0.15	5.35	0.09	2.43	0.09	0.17	4.00	3.70	0.16
Total	95.84	89.23	89.42	93.02	90.27	92.17	90.97	89.91	91.16	89.87	85.09

Note: (1–11) Sample numbers. In sample 578/4, we analyzed two (A, B) brownish globules (analyses, 1, 2, 4) with chlorite patches (analyses 3, 5) and an interlayer of brownish clayey rock (I, analysis 6) with chlorite patches (analyses 7, 8). In sample 578/3a (II), we analyzed the clayey matrix (analyses 9, 10) and chlorite segregations (analysis 11).

In sample 578/2, the biotite matrix of green pellets is suggested by their shape and certain features of the chemical composition. For example, comparison of pelletal and globular varieties of Al-glauconite shows that the pelletal phase is slightly enriched in Mg and Fe, relative to the globular variety (Table 9, analysis 3).

At the same time, sample 578/4 shows an opposite relationship: the green pellet is slightly enriched in Al, relative to the globular phase (Table 8, analysis 3; Table 4, analysis 4). This may be related to the composition of the weathered biotite in the sediment, the degree of its glauconitization, and other features.

Deep Catagenesis

In general, secondary alterations of sandy–silty rocks in the studied sections are typical of the deep catagenesis zone of platformal rocks. This is indicated by mosaic (conform-regeneration) and less common festoon-microstylolitic textures; the presence of authigenic quartz; the development of typical clay minerals (dioctahedral micas and trioctahedral Fe^{2+}–Mg-chlorite), which replace the matrix; the occurrence of clayey strata; the presence of brownish globules and/or brown pellets at some levels of the sections; as well as the predominance of authigenic chlorite in the mudstones.

Illitization of pellets. In sample 578/3e, two brown pellets, similar to biotite with respect to optical properties, are completely replaced by Fe-illite, as indicated by the sharp predominance of Al_2O_3 over Fe_2O_3 and sufficiently high K content (K_2O 7.25, 7.95%) in the minerals (Table 8, analyses 4, 5; Table 9). A similar pattern was also recorded for brown pellets in sample 566/3.

The mechanism of biotite transformation into the dioctahedral mica at the first stage of phase conversions is similar to the process of glauconitization in diagenesis (Ivanovskaya et al., 2003). Dioctahedral Fe–Al-micas are illitized during the subsequent catagenetic alterations. Such transformations are similar to those for the globular Al-glauconite (see below).

The illitization was probably faster in the green pellets with the highest Al content (Table 9).

Illitization of globules. In the studied samples, the degree of illitization is variable in both pelletal and globular varieties (up to complete pseudomorphs in some places). This process can postdate or predate chloritization (see below).

Dynamics of the chemical composition of different-color globules in thin sections of sample 578/4 (Table 4) shows that the Al_2O_3 content increases and the Fe_2O_3 content decreases during the gradual change from green to brownish green and brown color. Crystal chemistry of this process is as follows. Relative to the green variety (Table 3, formula 5), the brownish globules are characterized by higher contents of Al (Al_{VI} 1.02–1.49 f.u.) and lower contents of Fe (Fe_{VI}^{3+} 0.67–0.33 f.u.) in octahedral lattices of 2 : 1 layers of the micaceous mineral. In tetrahedral lattices, the tetrahedral charge is higher than the octahedral one because of the more intense replacement of Si by Al. Fe cations released from the structure are concentrated in the adjacent globules as hematite crystallites (and, possibly, amorphous phase), resulting in the brownish color of the globules.

The globular and pelletal glauconite could be illitized by either the solid-phase mechanism (with the retention of the micaceous matrix) or the mechanism of synthesis (solution–redeposition). In the fist case, the process is accompanied by the removal of Fe^{3+}, extraction of additional Al from the solutions and redistribu-

tion of this element along octahedral and tetrahedral sites. In the second case, glauconite particles are dissolved and Fe-illite particles are synthesized. However, the first mechanism is presumably preferable because of its higher efficiency in terms of energy consumption.

According to (Kopeliovich, 1965; Shutov et al., 1975; Nikolaeva, 1977; Drits and Kossovskaya, 1991; and others), transition from glauconite to the Al-rich varieties, i.e., aluminization (or illitization) with or without change in color of globules is caused by various processes. Illitization (aluminization) of the globular glauconite in Precambrian rocks is attributed to their intense postsedimentary alterations (Kopeliovich, 1965; Shutov et al., 1975) or specific conditions of the weathering of different-age glauconites (Nikolaeva, 1977; Drits and Kossovskaya, 1991). In the latter case, the grains are characterized by heterogeneous composition and structure (bleaching of grains, their patchy appearance, and formation of secondary ferruginous minerals).

It is interesting that Al-glauconite globules from sandstones of the Osorkhayata Formation (Lower Riphean, Olenek High) demonstrate zonality in color and composition. Microprobe data indicated that the bleached central portions of the globules are enriched in Al_2O_3 and depleted in Fe_2O_3, relative to their dark green margins. This is also supported by the electron diffraction data (b = 9.03 and 9.04 Å, respectively, for the pale and dark green sectors of the single grain). The bleaching of separate globules in the course of aluminization is fostered by deep catagenesis (Ivanovskaya et al., 1993).

Chloritization of pellets. Under conditions of insignificant chloritization, the brown Fe-illite pellets (samples 578/3e, 578/2) are depleted in K_2O, but enriched in MgO and total Fe (Table 8, analyses 6, 7) relative to the monomineral varieties (Table 8, analyses 4, 5). The more intense chloritization is recorded in one brown micaceous pellet from sample 566c. This is reflected in the lower concentration of K_2O and higher concentrations of FeO and MgO (Table 8, analysis 11). The chlorite composition fits the Fe^{2+}–Mg variety (Table 6, formula 5).

Brown pellets in samples 578/4 and 566/3 display interesting diffraction and/or composition patterns, suggesting an insignificant illitization or chloritization of the initial biotite. The affiliation of brown pellets to the chloritized and/or illitized biotite is primarily indicated by reflections in their diffractograms (sample 566/3; Figs. 6a–6c), as well as the quantitative (sample 578/4; Table 8, analyses 12, 13) and semiquantitative (sample 566/3) microprobe data, according to which Fe slightly prevails over Al and the K content is variable in the pellets.

It is well known that catagenesis promotes the transformation of biotite into the dioctahedral mica and trioctahedral chlorite. These processes were first studied by Kossovskaya et al. (1963, 1971) and confirmed by the subsequent investigations, including the high-precision methods (White et al., 1985; Aldahan and Morad, 1986; Drits and Kossovskaya, 1991; Ivanovskaya et al., 1993, 2003; Yapaskurt et al., 1999; and others).

Preservation of biotite is a rather rare phenomenon for the catagenetically altered glauconite-bearing rocks of the Precambrian, probably, because intensity and character of secondary alterations of even similar minerals in rocks can significantly vary not only in a single section, but also in a separate stratum.

Chloritization of brownish globules. This process is indicated in two Fe-illite globules (sample 578/4) by higher contents of Fe and MgO but lower contents of SiO_2 and K_2O (Table 7, analyses 1, 2). In turn, the chloritized globules are locally replaced by light green coarse-crystalline Fe^{2+}–Mg-chlorite (Table 5, analyses 3, 4; Table 6, formula 1). Fe-illite is also retained in one globule (Table 4, analysis 13).

Thus, the microprobe analysis of two brownish globules revealed the following phases: (1) Fe-illite; (2) blend of Fe-illite with the minor chlorite; and (3) monomineral Fe^{2+}–Mg-chlorite (Table 10, analyses 1–3, globules A) and globules without the Fe-illite phase (analyses 4, 5, globules B).

Based on semiquantitative analysis data, the brownish globules in thin sections of sample 578/4 are also characterized by a similar compositional variation. For example, margins of the brownish globule almost completely replaced by chlorite (Fig. 2b, light patches) are composed of both Fe-illite (analysis 39) and chlorite–illite blend dominated by the micaceous phase (analyses 36–38, 40). Dark patches in the globules are composed of the authigenic quartz.

Thus, globules in a single lamina (thin section) may be transformed according to two scenarios. In some globules, the process is restricted by illitization: Al-glauconite ($Al_{VI} > Fe_{VI}$) > Fe-illite ($Al_{VI} \gg Fe_{VI}$). In other globules, they are completely or partly transformed according to the following scheme: Al-glauconite > Fe-illite + Fe^{2+}–Mg-chlorite (fine-dispersed) > Fe^{2+}–Mg-chlorite (coarse-crystalline).

Chloritization of clayey strata and mudstones. Chlorite occurs as rather large segregations in the fine-dispersed component of brownish clayey strata (samples 578/4, 578/3e) composed of the blend of chlorite with a minor mica (Table 7, analysis 5; Fig. 2d). The chlorite makes up rather large patches that almost completely replace the strata in some places (Figs. 2a, 8c–8e). Mudstones are also almost completely replaced in samples 578/3a and 578/4b. The micaceous matrix is subordinate (Figs. 5c–5f, 9, 10).

Chlorite in the clayey matrix (sample 578/3e) is developed as large (from 3–6 to 10–20 μm) tabular hexagonal and/or irregular crystallites (Figs. 8c, 8d). Their distribution is subparallel, sheath-shaped, fan-shaped, and so on. They also make up spherulitic aggregates.

In mudstones (samples 578/3a, 578/4b), the groundmass consists of flakes of chlorite and micaceous minerals. Chlorite flakes are up to 8–15 μm in size (Figs. 9, 10). In sample 578/4b, chlorite flakes make up the characteristic concentric-zonal aggregates (Figs. 9d, 10a, 10b).

Chlorite probably formed in the brownish globules, clayey strata, and mudstones by the synthetic method, i.e., the dissolution of primary dioctahedral micaceous minerals and the growth of authigenic Fe^{2+}–Mg-chlorite crystals. In contrast, biotite and Fe-illite pellets were chloritized by the transformation mechanism with retention of the micaceous matrix. This is indicated by both literature data (Kossovsakya et al., 1963, 1971; Veblen and Ferry, 1983; Eggleton and Banfield, 1985; Drits and Kossovskaya, 1991; Yapaskurt et al., 1999; and others) and our high-precision analytical data (Ivanovskaya et al., 1989, 1993, 2003; Drits et al., 2001).

Data in Table 10 can illustrate the mechanism of chloritization (chemical aspect). For example, Al remains inert, contents of FeO and MgO increase, and contents of SiO_2 and K_2O decrease in the course of chloritization of both globules and rocks (including mudstones). SiO_2 is precipitated here as authigenic quartz (Fig. 2b), Fe^{3+} cations are removed from the structure to form hematite pellets. We recorded a similar pattern in the chloritization of the globular and pelletal Al-glauconite in sandstones of the Päräjarvi Formation (Upper Riphean, Srednii Peninsula) subjected to deep catagenesis (Ivanovskaya et al., 2003).

Compositions of Fe^{2+}–Mg-chlorites from different stratigraphic levels of the subformation show some discrepancies in contents of Fe and Mg (Table 5, analyses 3–15; Table 6, formulas 1–5), probably, owing to compositional variations in the initial substrate and/or changes in geochemical characteristics of solutions in enclosing rocks under high *PT* conditions. It is interesting that the chlorite composition in the thin section of sample 578/4 is virtually identical in globules, clayey strata, and interstitial cement (Table 5, analyses 3–6; Fig. 7).

In terms of the Fe index (Fe/Fe + Mg) versus the total content of Al cations ($Al_{tot} = Al_{IV} + Al_{VI}$) ratio in the crystallochemical classification scheme proposed by Drits and Kossovskaya (1991), data points of the studied chlorites fall into both the field of Fe^{2+}–Mg-chlorites of terrigenous rocks of deep catagenesis zone (samples 578/3e, 578/4) and the field adjacent to Fe-chlorites of iron ores (samples 578/3a, 578/4b).

Let us examine the process of almost complete chloritization of globules and brown pellets in sample 581b taken from the outer contact of diabase stock with glauconite-bearing rocks in the upper section of the subformation (Table 5, analyses 1, 2; Table 6, formulas 6, 7). Here, the pelletal and globular Fe^{2+}–Mg-chlorites are represented by varieties with a higher Mg content (Table 6, formulas 6, 7), relative to those in the deep catagenesis zone (formulas 1–5).

By analogy with previous results (Drits et al., 2001), we can assume that the chloritization pattern discussed above is related to the local heating and slight compositional alteration of pore waters that are enriched in Mg, relative to those in the glauconite-bearing siltstones beyond the stock intrusion zone.

Nearly all of the studied chlorite samples except sample 581 are characterized by polytype Ib ($\beta = 90°$) (Fig. 5f), in which the X-ray characteristics could not be identified because of the insufficient quantity of material. According to (Drits and Kossovskaya, 1991), polytype Ib is most widespread in the cement of unmetamorphosed sandstones. This structural type is also found in low-temperature hydrothermal veins, oolitic iron ores, and others.

We have detected chlorite of polytype Ib ($\beta = 90°$) not only in sandy–clayey rocks of the Arymas Formation, but also in globules and cement from gravelstones and sandstones of the Ust'-Il'ya Formation (Lower Riphean, Anabar Uplift) taken from the outer contact of a dike with glauconite-bearing rocks. Here, chlorite formed at ~170–230° (Drits et al., 2001).

According to (Ivanovskaya et al., 2003), chlorite is represented by polytype Ia ($\beta = 97°$) in globular and pelletal Al-glauconites from the catagenetically altered sandstones of the Päräjarvi Formation (Upper Riphean, Srednii Peninsula) (Ivanovskaya et al., 2003). The chlorite formed in deep catagenesis zone at a temperature not exceeding 100–150°C. It is believed that this polytype is least stable and transformed into the more stable polytype Ib ($\beta = 90°$) and IIb (Drits and Kossovskaya, 1991). As for chlorite of polytype Ib ($\beta = 90°$) from the Arymas Formation, they could hardly form at temperatures higher than those for chlorites of polytype Ia ($\beta = 97°$) from the Päräjarvi Formation. This is suggested by the universal presence of almost unaltered Al-glauconite grains in the studied sandy–silty rocks and by the preservation of biotite matrix in separate brown pellets at some levels of the section.

Regressive Catagenesis. Hypergenesis

Uplift of the study territory in the influence zone groundwaters provoked a slight local calcitization of rocks (Fig. 2d) and/or their ferrugination. This was also reflected in glauconite globules (Figs.3a–3d). For example, the brownish red color of glauconite grains in sample 578/8b is related to their replacement by hematite (Figs. 3c, 3d). However, they retained diffraction characteristics of the micaceous mineral.

In glauconitite (sample 566b), both processes are reflected, but the ferrugination is more prominent. Here, virtually all globules contain a certain amount of hematite (Figs.3a, 3b). Both globules and some portions of the rock were partly disintegrated at the stage of surface weathering. A part of the disintegrated mate-

rial was transported by formation waters. Another part was converted into a soft wet mass.

CONCLUSIONS

Globular phyllosilicates represented by hydromicas ($S > 1$) of the Al-glauconite composition (b = 9.036–9.06 Å) with different values of Fe index (Al_{VI} = 0.86–1.35 f.u., Fe^{3+}_{VI} = 0.40–0.85 f.u., n = 0.23–0.49) are ubiquitous in sandy–silty rocks of the lower subformation of the Arymas Formation.

At some levels of the studied section, deep catagenesis resulted in the illitization of glauconite globules and their brownish coloration. Moreover, some globules were chloritized at both microscopic and macroscopic levels. The globular Al-glauconite can be replaced according to the following schemes: (1) Al-glauconite ($Al_{VI} > Fe^{3+}_{VI}$) ⟶ Fe-illite ($Al_{VI} \gg Fe^{3+}_{VI}$); (2) Al-glauconite ⟶ Fe-illite + Fe^{2+}–Mg-chlorite (fine-dispersed) ⟶ Fe^{2+}–Mg-chlorite (coarse-crystalline). These processes can be observed in a single interlayer of the polished section.

The globular glauconite was probably illitized according to the solid-phase mechanism using the micaceous matrix, while the globular Fe-illites were chloritized by the synthetic method, i.e., dissolution of Fe-illite and growth of authigenic Fe^{2+}–Mg crystals.

The fine-dispersed and coarse-crystalline Fe^{2+}–Mg-chlorite also replaces the clayey strata and cement in the sandy–silty rocks. Mudstones are virtually completely replaced. The transformation takes place according to the synthetic mode (i.e., dissolution and redeposition).

The chlorites are commonly similar in composition and structure. They are represented by the trioctahedral Fe^{2+}–Mg variety of polytype Ib ($\beta = 90°$, b = 9.29–9.33 Å) with different contents of Fe and Mg.

Brown pellets of the primarily biotite composition are glauconitized in the course of diagenesis and illitized and/or chloritized in the course of catagenesis. The biotite matrix is sometimes retained during these transformations.

At the top of the lower subformation, globules and pellets were almost completely chloritized due to the local heating of glauconite-bearing siltstones at the outer contact of diabase stock. In such places, the Fe^{2+}–Mg-chlorite is characterized by the highest content of Mg.

Uplift of the territory in the influence zone of groundwaters promoted the development of calcitization and/or ferrugination (hematitization) of globules at some levels of the subformation. Moreover, glauconitites were disintegrated at the stage of surface weathering.

ACKNOWLEDGMENTS

The authors are grateful to V.A. Drits for critical remarks and consultations. We also thank N.K. Mirskaya and A.R. Geptner for help in the presentation of figures.

This work was supported by the Russian Foundation for Basic Research (project nos. 05-05-65290, 05-05-64135, and 06-05-64736) and the Presidium of the Russian Academy of Sciences (priority program no. 18).

REFERENCES

Aldahan, A.A. and Morad, S., Chemistry of Detrital Biotites and Their Phyllosilicate Intergrowths in Sandstones, *Clays Clay Miner.*, 1986, vol. 34, pp. 539–548.

Bailey, S.W., Chlorite: Structures and Crystal Chemistry, *Reviews Mineralogy*, 1988, vol. 19, pp. 347–403.

Drits, V.A. and Kossovskaya, A.G., Genetic Types of Dioctahedral Micas: Communication 1. Family of Iron–Magnesium Micas (Glauconites and Celadonites), *Litol. Polezn. Iskop.*, 1986, vol. 21, no. 5, pp. 19–33.

Drits, V.A. and Kossovskaya, A.G., *Glinistye mineraly: slyudy, khlority*, (Clay Minerals: Micas and Chlorites), Moscow: Nauka, 1991.

Drits, V.A., Kameneva, M.Yu., Sakharov, B.A., et al., *Problemy opredeleniya real'noi struktury glaukonitov i rodstvennykh tonkozernistykh fillosilikatov* (Issue of the Determination of the Real Structure of Glauconites and Cognate Fine-Grained Phyllosilicates), Novosibirsk: Nauka, 1993.

Drits, V.A., Ivanovskaya, T.A., Sakharov, B.A., et al., Pseudomorphous Replacement of Globular Glauconite by the Mixed-Layer Chlorite–Berthierine at the Outer Contact of Dike: Evidence from the Lower Riphean Ust'-Il'ya Formation, Anabar Uplift, *Litol. Polezn. Iskop.*, 2001, vol. 36, no. 4, pp. 390–407 [*Lithol. Miner. Resour.* (Engl. Transl.), 2001, vol. 36, no. 4, pp. 337–352].

Eggleton, R.A. and Banfield, J.F., The Alteration of Granitic Biotite to Chlorite, *Am. Miner.*, 1985, vol. 70, nos. 9/10, pp. 902–910.

Fenoshina, U.I., Glauconite from Lower Tortonian Deposits of the Lyuben Health Resort, in *Voprosy mineralogii osadochnykh obrazovanii* (Issues of the Mineralogy of Sedimentary Rocks), Lvov: Lvov. Gos. Univ., 1961, part 6, pp. 226–282.

Galliher, E.W., Glauconite Genesis, *Bull. Geol. Soc. Am.*, 1935, vol. 46, pp. 1351–1366.

Geokhronologiya dokembriya Sibirskoi platformy i ee skladchatogo obramleniya (Precambrian Geochronology of the Siberian Craton and Its Folded Framing), Leningrad: Nauka, 1968.

Geptner, A.R. and Ivanovskaya, T.A., Glauconite from Lower Cretaceous Marine Terrigenous Rocks of England: A Concept of Biochemogenic Origin, *Litol. Polezn. Iskop.*, 2000, vol. 35, no. 5, pp. 487–499 [*Lithol. Miner. Resour.* (Engl. Transl.), 2000, vol. 35, no. 5, pp. 434–444].

Gorokhov, I.M., Yakovleva, O.V., Semikhatov, M.A., et al., "Rejuvenated" Al-glauconite in Vendian–Cambrian Deposits of Podolian Dniester Region, Ukraine: Rb–Sr and K-Ar Systematics and ^{57}Fe Mössbauer Spectra, *Litol. Polezn. Iskop.*, 1997, vol. 32, no. 6, pp. 616–635 [*Lithol. Miner. Resour.* (Engl. Transl.), 1997, vol. 32, no. 6, pp. 541–558].

Ivanovskaya, T.A., Globular Phyllosilicates of the Glauconite–Illite Composition in Rocks of the Debengda Formation (Middle Riphean, Olenek Uplift), *Litol. Polezn. Iskop.*, 1994, vol. 29, no. 6, pp. 101–113.

Ivanovskaya, T.A., Glauconite–Illite Minerals in Upper Vendian–Lower Cambrian Boundary Deposits of Podolia, Dniester Region, *Litol. Polezn. Iskop.,* 1996, vol. 31, no. 6, pp. 509–601 [*Lithol. Miner. Resour.* (Engl. Transl.), 1996, vol. 31, no. 6, pp. 524–534].

Ivanovskaya, T.A. and Geptner, A.R., Glauconite at Different Stages of Lithogenesis in Lower Cambrian Rocks of Western Lithuania, *Litol. Polezn. Iskop.,* 2004, vol. 39, no. 3, pp. 227–240 [*Lithol. Miner. Resour.* (Engl. Transl.), 2004, vol. 39, no. 3, pp. 191–202].

Ivanovskaya, T.A., Tsipurskii, S.I., and Yakovleva, O.V., Mineralogy of Globular Phyllosilicates from Riphean and Vendian of Siberia and the Urals, *Litol. Polezn. Iskop.*, 1989, vol. 24, no. 3, pp. 83–99.

Ivanovskaya, T.A., Tsipurskii, S.I., and Yakovleva, O.V., Lower Cambrian Globular Phyllosilicates in Northern Estonia, *Litol. Polezn. Iskop.,* 1991, vol. 26, no. 4, pp. 120–127.

Ivanovskaya, T.A., Kats, A.G., Florova, Z.B., et al., Structure, Lithology, and Mineralogy of the Basal Part of the Lower Riphean in the Olenek Uplift (Osorkhayata Formation), *Stratigr. Geol. Korrelyatsiya*, 1993, vol. 1, no. 4, pp. 84–92.

Ivanovskaya, T.A., Sakharov, B.A., Gorkova, N.V., et al., Berthierine in Catagenetically Altered Vendian–Cambrian Deposits of Podolia, Dniester Region, *Litol. Polezn. Iskop.*, 1999, vol. 34, no. 2, pp. 198–212 [*Lithol. Miner. Resour.* (Engl. Transl.), 1999, vol. 34, no. 2, pp. 170–183].

Ivanovskaya, T.A., Gor'kova, N.V., Karpova, G.V., et al., Chloritization of Globular and Platy Phyllosilicates of the Glauconite Series in Terrigenous Rocks of the Upper Riphean Päräjarvi Formation, Srednii Peninsula, *Litol. Polezn. Iskop.*, 2003, vol. 38, no. 6, pp. 584–598 [*Lithol. Miner. Resour.* (Engl. Transl.), 2003, vol. 38, no. 6, pp. 495–508].

Kats, A.G. and Florova, Z.B., New Data on the Upper Paleozoic Stratigraphy of the Southern Slope of the Olenek Uplift, in *Pozdnii dokembrii i rannii paleozoi Sibiri. Sibirskaya platforma i vneshnyaya zona Altae-Sayanskoi skladchatoi oblasti* (Late Precambrian and Early Paleozoic of Siberia: Siberian Craton and External Zone of the Altai–Sayan Foldbelt), Novosibirsk: Inst. Geol. Geokhim. Sib. Otd. Akad. Nauk SSSR, 1986, pp. 65–84.

Komar, V.A., *Stromatolity verkhnedokembriiskikh otlozhenii severa Sibirskoi platformy i ikh stratigraficheskoe znachenie* (Stromatolites from Upper Precambrian Deposits of Northern Siberian Craton and Their Stratigraphic Implications), Moscow: Nauka, 1966.

Kopeliovich, A.V., *Epigenez drevnikh tolshch yugo-zapada Russkoi platformy*, (Epigenesis of Ancient Sequences in the Southwestern Russian Platform), Moscow: Nauka, 1965.

Kossovskaya, A.G., Drits, V.A., and Aleksandrova, V.A., The History of Trioctahedral Micas in Sedimentary Rocks, *Litol. Polezn. Iskop.*, 1963, no. 2, pp. 178–196.

Kossovskaya, A.G., Drits, V.A., and Sokolova, T.N., Specific Features of the Formation of Clay Minerals in Various Facies–Climatic Environments, in *Epigenez i ego mineral'nye indikatory* (Epigenesis and Its Mineral Indicators), Moscow: Nauka, 1971, pp. 35–54.

Micas. Reviews in Mineralogy, Bailey, S.W., Ed., 1984, vol. 13.

Millot, G., *Geology of Clays. Weathering, Sedimentology, Geochemistry*, Paris: Springer, 1965. Translated under the title *Geologiya glin (vyvetrivanie, sedimentologiya, geokhimiya)*, Leningrad: Nedra, 1968.

Mineraly. Spravochnik, (Minerals: Reference Book), Moscow: Nauka, 1992, vol. 4, nos. 1/2.

Murav'ev, V.I., Epigenetic Alterations of Mesozoic Rocks in the Southeastern Russian Platform, *Izv. Akad. Nauk SSSR, Ser. Geol.*, 1962, no. 6, pp. 34–47.

Nikolaeva, I.V., *Mineraly gruppy glaukonita v osadochnykh formatsiyakh* (Glauconite Group Minerals in Sedimentary Formations), Novosibirsk: Nauka, 1977.

Rentgenografiya osnovnykh tipov porodoobrazuyushchikh mineralov (sloistye i karkasnye silikaty) (The X-Ray Diffraction Analysis of Major Types of Rock-Forming Minerals: Layer and Framework Silicates), Leningrad: Nedra, 1983.

Semikhatov, M.A. and Serebryakov, S.N., *Sibirskii gipostratotip rifeya* (Siberian Hypostratotype of the Riphean), Moscow: Nauka, 1983.

Semikhatov, M.A., Gorokhov, I.M., Ivanovskaya, T.A., et al., K–Ar and Rb–Sr Dating of Riphean and Cambrian Globular Phyllosilicates in the USSR: Materials for the Geochronometer Evaluation, *Litol. Polezn. Iskop.*, 1987, vol. 22, no. 5, pp. 78–96.

Shenfil, V.Yu., *Pozdnii dokembrii Sibirskoi platformy* (Late Precambrian of the Siberian Craton), Novosibirsk: Nauka, 1991.

Shenfil, V.Yu., Yakshin, M.S., Kats, A.G., and Florova, Z.B., Detailed Subdivision of the Upper Part of Riphean Sequence in the Olenek Uplift, in *Pozdnii dokembrii i rannii paleozoi Sibiri. Rifei i vend* (Late Precambrian and Early Paleozoic of Siberia: Riphean and Vendian), Novosibirsk: Nauka, 1988, pp. 20–35.

Shpunt, B.R., Shapovalova, I.G., and Shamshina, E.A., *Pozdnii dokembrii severa Sibirskoi platformy* (Late Precambrian of the Northern Siberian Craton), Novosibirsk: Nauka, 1982.

Shutov, V.D., Formation Model of Globular Glauconite and "Scolite" with Reference to the Scole Deposit, *Litol. Polezn. Iskop.*, 1984, vol. 19, no. 1, pp. 147–152.

Shutov, V.D., Kats, M.Ya., Drits, V.A., et al., Crystallochemistry of Glauconite as an Indicator of Depositional Environment and Postsedimentary Alteration, in *Kristallokhimiya*

mineralov i geologicheskie problemy (Crystallochemistry of Minerals and Geological Problems), Moscow: Nauka, 1975, pp. 74–81.

Thompson, J.A. and Hower, J., The Mineralogy of Glauconite, *Clays Clay Miner.*, 1975, vol. 23, pp. 284–300.

Triplehorn, D.M., Morphology, Internal Structure and Origin of Glauconite Pellets, *Sedimentology,* 1966, vol. 6, no. 4, pp. 247–266.

Tsipurskii, S.I., Ivanovskaya, T.A., Sakharov, B.A., et al., Nature of the Coexistence of Glauconite, Fe-Illite, and Illite in Globular Micaceous Minerals from Various Lithological and Age Types of Rocks, *Litol. Polezn. Iskop.*, 1992, vol. 27, no. 5, pp. 65–75.

Veblen, D.K. and Ferry, J.M., A TEM Study of the Biotite-Chlorite Reaction and Comparison with Petrological Observations, *Am. Miner.,* 1983, vol. 68, pp. 1160–1168.

White, S.H., Hugget, J.M., and Shaw, H.F., Electron Optical Studies of Phyllosilicate Intergrowths in Sedimentary and Metamorphic Rocks, *Miner. Mag.*, 1985, vol. 49, pp. 413–423.

Yapaskurt, O.V., Parfenova, O.V., Kosorukov, V.L., and Sukhov, A.V., Genesis and Stadial Transformations of Micas and Chlorides under Various Geodynamic Conditions of Lithogenesis, *Vestn. Mosk. Gos. Univ., Ser. 4: Geol.*, 1999, no. 5, pp. 3–12.

Zaitseva, T.S., Gorokhov, I.M., Ivanovskaya, T.A., et al., Mineralogy, Mössbauer Characteristics, and K–Ar Isotopic Age of Glauconite from the Lower Cambrian Sediments, Western Lithuania, *Litol. Polezn. Iskop.*, 2005, vol. 40, no. 4, pp. 403–415 [*Lithol. Miner. Resour.* (Engl. Transl.), 2005, vol. 40, no. 4, pp. 353–363].